THE EUROPEAN
PHYSICAL JOURNAL C

NLO QCD corrections to off-shell $t\bar{t}W^{\pm}$ production at the LHC: correlations and asymmetries

Giuseppe Bevilacqua[1,a], **Huan-Yu Bi**[2,b], **Heribertus Bayu Hartanto**[3,c], **Manfred Kraus**[4,d], **Jasmina Nasufi**[2,e], **Malgorzata Worek**[2,f]

[1] MTA-DE Particle Physics Research Group, University of Debrecen, PBox 105, 4010 Debrecen, Hungary
[2] Institute for Theoretical Particle Physics and Cosmology, RWTH Aachen University, 52056 Aachen, Germany
[3] Cavendish Laboratory, University of Cambridge, J.J. Thomson Avenue, Cambridge CB3 0HE, UK
[4] Physics Department, Florida State University, Tallahassee, FL 32306-4350, USA

Abstract Recent discrepancies between theoretical predictions and experimental data in multi-lepton plus b-jets analyses for the $t\bar{t}W^{\pm}$ process, as reported by the ATLAS collaboration, have indicated that more accurate theoretical predictions and high precision observables are needed to constrain numerous new physics scenarios in this channel. To this end we employ NLO QCD computations with full off-shell top quark effects included to provide theoretical predictions for the $\mathcal{R} = \sigma_{t\bar{t}W^+}/\sigma_{t\bar{t}W^-}$ cross section ratio at the LHC with $\sqrt{s} = 13$ TeV. Depending on the transverse momentum cut on the b-jet we obtain 2–3% theoretical precision on $\mathcal{R}$, which should help to shed some light on new physics effects that can reveal themselves only once sufficiently precise Standard Model theoretical predictions are available. Furthermore, triggered by these discrepancies we reexamine the charge asymmetry of the top quark and its decay products in the $t\bar{t}W^{\pm}$ production process. In the case of charge asymmetries, that are uniquely sensitive to the chiral nature of possible new physics in this channel, theoretical uncertainties below 15% are obtained. Additionally, the impact of the top quark decay modelling is scrutinised by explicit comparison with predictions in the narrow-width approximation.

1 Introduction

The Large Hadron Collider (LHC) with the Run II energy of $\sqrt{s} = 13$ TeV has opened up the possibility of studying various top quark production and decay mechanisms at larger mass scales than previously explored in any experiment. The $t\bar{t}$ pair production associated with the $W^{\pm}$ gauge boson is among the most interesting signatures that can be studied with high precision at the LHC. It is a key process to constrain top quark intrinsic properties, which might be modified in the presence of new physics. Moreover, the process can be used in the framework of the Standard Model Effective Field Theory (SMEFT), where the effects of potential new particles can be systematically included in terms of higher-dimensional operators, see e.g. [1–5]. The latter are suppressed by a sufficiently large new physics energy scale Λ. The framework relies on the idea that new physics is too heavy to be directly produced and observed at the LHC, thus, only deviations from the Standard Model (SM) can be probed in various ATLAS and CMS top quark measurements. Compared with top quark pair production and single top quark production, the associated $t\bar{t}W^{\pm}$ process does not bring sensitivity to new operators, however, it helps to resolve blind directions in the SMEFT parameter space that occur in the current LHC fits. On top of that $t\bar{t}W^{\pm}$ can probe operators that are difficult to access in other channels. For example, since the $W^{\pm}$ gauge boson is radiated from the initial state, $t\bar{t}W^{\pm}$ is sensitive to a subset of the possible four-quark operators only. In the SM, $t\bar{t}W^{\pm}$ is dominated by quark–antiquark interactions, while $t\bar{t}$ is dominated by the gg initial state. This means that relative to the SM contribution the four-quark operators would give sizeable effects in the $t\bar{t}W^{\pm}$ production process. Consequently, $t\bar{t}W^{\pm}$ production is often included in

[a] e-mail: giuseppe.bevilacqua@science.unideb.hu

[b] e-mail: bihy@physik.rwth-aachen.de

[c] e-mail: hbhartanto@hep.phy.cam.ac.uk

[d] e-mail: mkraus@hep.fsu.edu

[e] e-mail: jasmina.nasufi@rwth-aachen.de

[f] e-mail: worek@physik.rwth-aachen.de (corresponding author)

the global SMEFT analysis of LHC top quark measurements, see e.g. Ref. [6].

In addition, the $t\bar{t}W^{\pm}$ process plays an important role in studies of the top quark charge asymmetry denoted as A_c^t [7,8]. Also in this case the lack of the symmetric gg initial state and the emission of the $W^{\pm}$ gauge boson from the initial states contribute to a substantially larger top quark charge asymmetry than that measured in the $t\bar{t}$ process. Furthermore, the asymmetry of the top quark decay products, i.e the charged lepton (A_c^{ℓ}) and the b-jet (A_c^b) are very large and already present at the LO due to the polarisation of the initial fermionic line by the $W^{\pm}$ emission. These asymmetries are an interesting playground for various beyond the SM (BSM) theories, as A_c^t, A_c^{ℓ} and A_c^b are uniquely sensitive to the chiral nature of possible new physics that might directly affect such measurements.

Last but not least, $t\bar{t}W^{\pm}$ production is a background process in the multi-lepton final state with two same-sign leptons, accompanied by missing transverse momentum and b-jets [9–12]. Even though same-sign leptons are a relatively rare phenomenon in the SM, as they only appear in processes with a rather small cross section, they have been extensively exploited in various models of new physics. The same-sign lepton signature is present, among others, in models with supersymmetry, universal extra dimensions, top-quark partners and an extended Higgs boson sector [13–23]. Besides, same-sign leptons are considered a key feature in searches for heavy Majorana neutrinos as well as for tt and $\bar{t}\bar{t}$ resonances [24,25].

Finally, the $pp \to t\bar{t}W^{\pm}$ process is the main background in SM measurements involving final states with multiple leptons and b-jets. This is the case, for example, for the measurement of the associated production of the SM Higgs boson with top quarks [26]. The $pp \to t\bar{t}W^{\pm}$ process has also played a crucial role in the announcement of strong evidence for the production of four top quarks, an analysis, which has been recently performed by the ATLAS Collaboration [27].

The direct measurement of $pp \to t\bar{t}W^{\pm}$ production in multi-lepton final states has already been carried out at $\sqrt{s} = 13$ TeV by the ATLAS and CMS collaborations [28–30]. In the recent measurements of $t\bar{t}H$ and $t\bar{t}W^{\pm}$ production in multi-lepton final states [26] the resulting $t\bar{t}W^{\pm}$ normalisation has been found to be higher than the theoretical prediction provided by multipurpose Monte Carlo (MC) generators, which are currently employed by the ATLAS collaboration. Apart from the $t\bar{t}W^{\pm}$ normalisation, a tension in the modelling of the final state kinematics in the phase space regions dominated by $t\bar{t}W^{\pm}$ production, has been observed. From the experimental point of view such an accurate study of $pp \to t\bar{t}W^{\pm}$ production in the same-sign lepton final state has become feasible thanks to the increasing amount of data collected at the LHC with $\sqrt{s} = 13$ TeV. This increased integrated luminosity has significantly raised

the need for more precise theoretical predictions. The latter should include higher order QCD corrections both to the production and decays of top quarks and W gauge bosons as well as $t\bar{t}$ spin correlations at the same level of accuracy.

The first calculations for the $pp \to t\bar{t}W^{\pm}$ process, that meet the mentioned conditions, have been carried out in the narrow-width approximation (NWA) within the MCFM framework [31]. The first full NLO QCD computations, which include complete top quark off-shell effects for the $pp \to t\bar{t}W^{\pm}$ process in the multi-lepton channel, have been recently presented in Ref. [32]. In these computations, obtained with the help of HELAC- NLO, off-shell top quarks have been described by Breit–Wigner propagators, furthermore, double-, single- as well as non-resonant top-quark contributions along with all interference effects have been consistently incorporated at the matrix element level. Independent computations for $t\bar{t}W^+$ production have been obtained very recently within the MOCANLO+RECOLA framework [33]. They not only confirmed the results presented in Ref. [32] but also performed a comparison between the full results and those obtained with the help of the double-pole approximation.

In Ref. [32] results at NLO QCD accuracy have been presented in the form of fiducial integrated and differential cross sections for two selected renormalisation and factorisation scale choices (a fixed and a dynamical one) and three different PDF sets. Detailed studies of the scale dependence of the NLO predictions have been carried out together with calculations of PDF uncertainties. Furthermore, the impact of the top quark off-shell effects on the $pp \to t\bar{t}W^{\pm}$ cross section has been examined by an explicit comparison with the results in the NWA. In the current paper we will move away from the technical aspects of higher order calculations and the estimation of the residual theoretical uncertainties and go towards more phenomenological studies for the $pp \to t\bar{t}W^{\pm}$ process. Specifically, the purpose of this paper is twofold. First, we would like to provide a systematic analysis of the two processes $pp \to t\bar{t}W^+$ and $pp \to t\bar{t}W^-$ in the multi-lepton decay channel to extract the most accurate NLO QCD predictions for the $\mathcal{R} = \sigma_{t\bar{t}W^+}^{\text{NLO}}/\sigma_{t\bar{t}W^-}^{\text{NLO}}$ cross section ratio. Generally, cross section ratios are more stable against radiative corrections than absolute cross sections, assuming that the two processes are correlated. They have smaller theoretical uncertainties as various uncertainties tend to cancel in a cross section ratio. Consequently, such precise theoretical predictions have enhanced predictive power and should be used in indirect searches for new physics at the LHC. Let us add here, that the $\mathcal{R} = \sigma_{t\bar{t}W^+}^{\text{NLO}}/\sigma_{t\bar{t}W^-}^{\text{NLO}}$ cross section ratio has recently been studied in Ref. [34] in the context of parton shower. The NLO QCD and subleading electroweak corrections for the $t\bar{t}W^{\pm}$ process were matched, using the MC@NLO matching scheme [35,36], to the parton shower using the PYTHIA8 framework [37] and the MADGRAPH5_AMC@NLO system

[38,39]. The top quark and the $W^\pm$ gauge boson decays were realised within the MADSPIN framework [40] in order to fully keep the LO spin correlations. The $\mathcal{R}$ ratio has been considered for the two following signatures: the same sign di-lepton and the multi lepton channels. The scale uncertainties were taken to be correlated, although, correlations were not studied in any detail. In addition, the PDF uncertainties were not discussed at all.

The second goal of the paper is to study separately the intrinsic properties of $t\bar{t}W^+$ and $t\bar{t}W^-$ production. More specifically, we shall use state-of-the-art NLO QCD theoretical predictions for the $t\bar{t}W^\pm$ process to re-examine the top quark charge asymmetry and asymmetries of the top quark decay products both at the integrated and differential level. Likewise, in this case, the polarisation and asymmetry effects in the $pp \rightarrow t\bar{t}W^\pm$ production process can be employed to constrain new physics effects that might occur in this channel. Furthermore, for both the cross section ratio and the top quark (decay products) charge asymmetry, the impact of the modelling of top quark production and decays will be studied.

We note here, that state-of-the art theoretical predictions at NLO in QCD with complete top quark off-shell effects included are also available for other processes at the LHC. Such effects, for example, have been incorporated for $pp \rightarrow t\bar{t}$ [41–44], $pp \rightarrow t\bar{t}j$ [45,46], $pp \rightarrow t\bar{t}H$ [47], $pp \rightarrow t\bar{t}\gamma$ [48] and for $t\bar{t}Z(Z \rightarrow \nu_\ell \nu_\ell)$ [49]. They have also been incorporated for the $pp \rightarrow t\bar{t}b\bar{b}$ process [50]. We additionally add, that continuous efforts have been devoted to improve the theoretical modeling of hadronic observables for $t\bar{t}W^\pm$ at NLO through matching with parton shower and multi-jet merging [34,51–53]. A further step towards a more precise modelling of on-shell $t\bar{t}W^\pm$ production with stable top quarks and $W^\pm$ gauge boson has been achieved by including either NLO electroweak corrections [54] and the subleading electroweak corrections [55,56] or by incorporating soft gluon resummation effects with next-to-next-to-leading logarithmic accuracy [57–61]. Very recently, NLO QCD and electroweak corrections to the full off-shell $t\bar{t}W^+$ production at the LHC have been combined for the first time for the three-charged-lepton channel [62].

The paper is organised as follows. In Sect. 2 the HELAC-NLO computational framework and input parameters used in our studies are briefly described. In Sect. 3 correlations between $t\bar{t}W^+$ and $t\bar{t}W^-$ are examined. The results for the cross section ratio $\mathcal{R} = \sigma_{t\bar{t}W^+}^{\rm NLO}/\sigma_{t\bar{t}W^-}^{\rm NLO}$ are provided in Sect. 4. The integrated top quark charge asymmetry as well as asymmetries of the top quark decay products are studied in Sect. 5. Results for the differential and cumulative A_c^ℓ asymmetry are provided in Sect. 6. In Sect. 7 the results are summarised and our conclusions are provided. Finally, in appendix A we discuss the Kolmogorov–Smirnov test that may be used to

provide a quantitative measure of similarity between the two given processes.

2 Computational framework and input parameters

All our results both for the full off-shell and NWA computations have been obtained with the help of the HELAC-NLO Monte Carlo framework [63]. The calculation was performed using HELAC-1LOOP [64,65] for the virtual corrections and HELAC-DIPOLES [66,67] for the real emission part. The integration over the phase space has been achieved with the help of KALEU [68]. In our studies we keep the Cabibbo–Kobayashi–Maskawa mixing matrix diagonal and neglect the Higgs boson contributions. Following recommendations of the PDF4LHC Working Group for the usage of PDFs suitable for applications at the LHC Run II [69] we employ the NNPDF3.0 PDF set [70]. In particular, we use `NNPDF30-nlo-as-0118` with $\alpha_s(m_Z) = 0.118$ (`NNPDF30-lo-as-0130` with $\alpha_s(m_Z) = 0.130$) at NLO (LO). The running of the strong coupling constant α_s with two-loop accuracy at NLO is provided by the LHAPDF interface [71]. The number of active flavours is set to $N_F = 5$. We employ the following SM input parameters

$$
\begin{aligned}
&G_\mu = 1.166378 \times 10^{-5}\,{\rm GeV}^{-2}\,, & &m_t = 172.5\,{\rm GeV}\,, \\
&m_W = 80.385\,{\rm GeV}\,, & &\Gamma_W^{\rm NLO} = 2.09767\,{\rm GeV}\,, \\
&m_Z = 91.1876\,{\rm GeV}\,, & &\Gamma_Z^{\rm NLO} = 2.50775\,{\rm GeV}\,, \\
&\Gamma_t^{\rm NLO} = 1.33247\,{\rm GeV}\,, & &\Gamma_{t,{\rm NWA}}^{\rm NLO} = 1.35355\,{\rm GeV}\,.
\end{aligned}
$$

(1)

For the W and Z gauge boson widths we use the NLO QCD values as calculated for $\mu_R = m_W$ and $\mu_R = m_Z$ respectively. All other partons, including bottom quarks, as well as leptons are treated as massless particles. The LO and NLO top quark widths are calculated according to Ref. [43]. The top quark width is treated as a fixed parameter throughout this work. Its value corresponds to a fixed scale $\mu_R = m_t$. The electromagnetic coupling α is calculated from the Fermi constant G_μ, i.e. in the G_μ−scheme, via

$$
\alpha_{G_\mu} = \frac{\sqrt{2}}{\pi}\,G_\mu\,m_W^2\,\sin^2\theta_W\,,
$$

(2)

where $\sin^2\theta_W$ is defined according to

$$
\sin^2\theta_W = 1 - \frac{m_W^2}{m_Z^2}\,.
$$

(3)

We use kinematic-dependent factorisation and renormalisation scales $\mu_R = \mu_F = \mu_0$ with the central value $\mu_0 = H_T/3$ where H_T is the scalar sum of all transverse momenta in the event, including the missing transverse momentum.

The latter is constructed from the three neutrinos ν_e, ν_e and ν_μ. The additional light jet, if resolved, is not included in the definition of H_T. In various comparisons we also use a fixed scale defined as $\mu_0 = m_t + m_W/2$. Jets are constructed out of all final-state partons with pseudo-rapidity $|\eta| < 5$ via the $anti-k_T$ jet algorithm [72] with the separation parameter $R = 0.4$. We require exactly two b-jets and three charged leptons, two of which are same-sign leptons. All final states have to fulfill the following selection criteria that mimic very closely the ATLAS detector response [26]

$$p_{T,\ell} > 25\,\mathrm{GeV}\,, \qquad p_{T,b} > 25\,\mathrm{GeV}\,,$$
$$|y_\ell| < 2.5\,, \qquad\qquad |y_b| < 2.5\,, \qquad (4)$$
$$\Delta R_{\ell\ell} > 0.4\,, \qquad\qquad \Delta R_{\ell b} > 0.4\,,$$

where ℓ stands for the charged lepton. We do not impose any restrictions on the kinematics of the additional light jet and the missing transverse momentum.

3 Correlations between $t\bar{t}W^+$ and $t\bar{t}W^-$

We start with the NLO QCD differential cross sections for $pp \to e^+\nu_e\,\mu^-\bar{\nu}_\mu\,e^+\nu_e\,b\bar{b} + X$ and $pp \to e^-\bar{\nu}_e\,\mu^+\nu_\mu\,e^-\bar{\nu}_e$ $b\bar{b} + X$. They are obtained for the LHC Run II energy of $\sqrt{s} = 13$ TeV. For brevity, we will refer to these reactions as $pp \to t\bar{t}W^+$ and $pp \to t\bar{t}W^-$. In Ref. [32] we have shown that the NLO QCD effects for $t\bar{t}W^+$ and $t\bar{t}W^-$ are very similar. Indeed, both processes show alike $\mathcal{K}$-factors and dependencies on the perturbative scales. Furthermore, the off-shell effects for both processes are of the same order. Thus, it is highly probable that some of the uncertainties cancel in the ratio of $t\bar{t}W^+$ and $t\bar{t}W^-$ cross sections, and $\mathcal{R} = \sigma^{\mathrm{NLO}}_{t\bar{t}W^+}/\sigma^{\mathrm{NLO}}_{t\bar{t}W^-}$ might exhibit an enhanced perturbative stability. In the following we would like to understand similarities and potential differences between the two processes even further. We note that, at the leading order the production mechanism for $t\bar{t}W^+$ ($t\bar{t}W^-$) is via the scattering of up-type quark (anti-quark) and the corresponding down-type anti-quark (quark), i.e. $u\bar{d}$ and $c\bar{s}$ for $pp \to t\bar{t}W^+$ as well as $\bar{u}d$ and $\bar{c}s$ for $pp \to t\bar{t}W^-$. The quark–gluon initial state opens up only at NLO in QCD. Similarities with respect to higher order QCD corrections, in the production mechanisms as well as in the kinematics of the final states suggest that the two processes may be treated as correlated as far as the choice of scales is concerned. In any case, as long as one is interested in some specific observables listed below. To show this we examine the common features in the kinematics of the final states. Since we are interested in the shape differences/similarities only and because the fiducial cross section for $pp \to t\bar{t}W^-$ is about a factor of two smaller than the one for the $pp \to t\bar{t}W^+$ process we concentrate on the normalised NLO QCD differential cross sections.

In the following the collection of leptonic observables will be examined. In the $pp \to t\bar{t}W^\pm$ process same-sign charged leptons $e^\pm e^\pm$ occur. In the case of final states with identical leptons the ordering in p_T has to be introduced to label the particles. To this end, we denote the first and the second hardest same-sign charged lepton as $e^\pm_1$ and $e^\pm_2$ respectively. In Fig. 1 we present the NLO QCD differential cross sections for $pp \to t\bar{t}W^+$ and $pp \to t\bar{t}W^-$ as a function of the transverse momentum of $e^\pm_1$ (p_{T,e_1}), the invariant mass of the $e^\pm_1 e^\pm_2$ system (M_{e_1,e_2}) and the scalar sum of the transverse momenta of the charged leptons available in the given process (H^{lep}_T). The latter is defined as

$$H^{lep}_T = p_{T,\mu^\mp} + p_{T,e^\pm_1} + p_{T,e^\pm_2}\,. \qquad (5)$$

Also shown in Fig. 1 is the distance in the azimuthal angle rapidity plane between $e^\pm_1$ and $e^\pm_2$ ($\Delta R_{e_1,e_2}$). All differential cross sections shown are, indeed, rather similar. This is particularly true for H^{lep}_T, $\Delta R_{e_1,e_2}$ and p_{T,e_1} but also for M_{e_1,e_2} at the beginning of the spectrum. Even-though the latter distribution diverges substantially in the tails, the contribution from these particular phase-space regions to the integrated fiducial $pp \to t\bar{t}W^\pm$ cross section is negligible. To contrast these results, we refer the reader to Ref. [73] where the processes $pp \to t\bar{t}b\bar{b}$ and $pp \to t\bar{t}jj$ demonstrate sizeable dissimilarities over the whole kinematics range.

In the next step we look at the b-jet kinematics. The two b-jets are ordered according to their p_T. The hardest (b_1) and the softest b-jet (b_2) kinematics are exhibited in Fig. 2. We note here, however, that the charge identification of the b-jets is possible at the LHC, see e.g [74–77]. Thus, one can distinguish between b-jets initiated by b and $\bar{b}$. In this work, however, we do not perform such b-jet identification. We depict the NLO QCD differential cross sections as a function of the transverse momentum of b_1 (p_{T,b_1}), the invariant mass of the two b-jet system (M_{b_1,b_2}) and the distance in the azimuthal angle rapidity plane between b_1 and b_2 ($\Delta R_{b_1,b_2}$). Also presented in Fig. 2 is the scalar sum of the transverse momenta of all the visible final states, denoted as H^{vis}_T. The latter is given by

$$H^{vis}_T = p_{T,b_1} + p_{T,b_2} + p_{T,\mu^\mp} + p_{T,e^\pm_1} + p_{T,e^\pm_2}\,. \qquad (6)$$

An interesting comment can be made here. Namely, that the b-jets are preferably produced in back-to-back configurations. Hereby, b-jets come more often from top quark decays rather than from the $g \to b\bar{b}$ splitting. The latter configuration, which is produced in the off-shell case where no top-quark resonances are present, would manifest itself in the enhancement close to $\Delta R_{b_1,b_2} \approx 0.4$. In the case of b-jet kinematics and for the H^{vis}_T observable we can see similarities between $pp \to t\bar{t}W^+$ and $pp \to t\bar{t}W^-$.
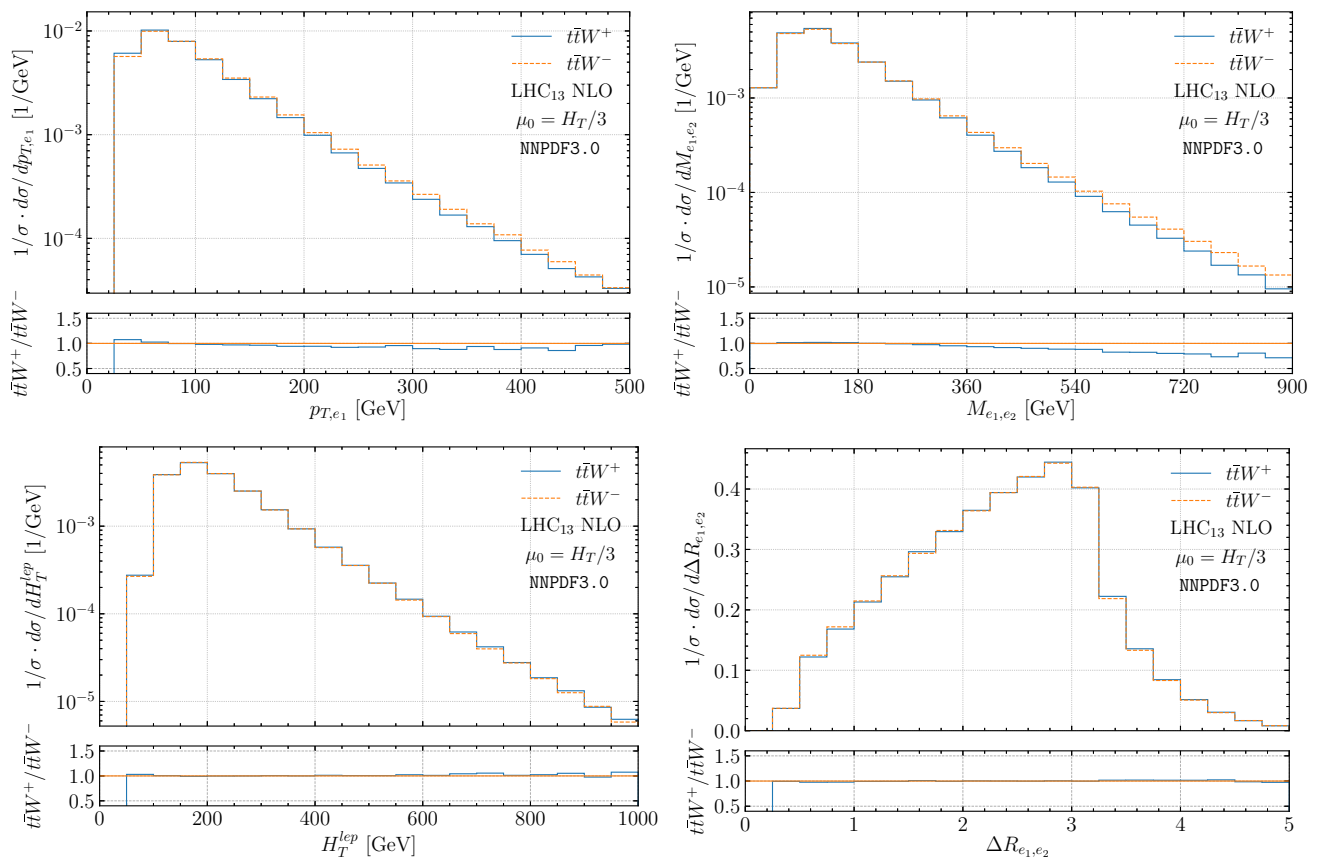
Fig. 1 Comparison of the normalised NLO QCD differential cross sections for $pp \rightarrow t\bar{t}W^\pm$ in the multi-lepton final state at the LHC with $\sqrt{s} = 13$ TeV. The transverse momentum of the hardest same-sign lepton (p_{T,e_1}) and the invariant mass of the two same-sign leptons ($M_{e_1 e_2}$) are presented. Also given are the scalar sum of the transverse momenta

of the leptons (H_T^{lep}) and the distance in the azimuthal angle rapidity plane between the two same-sign leptons ($\Delta R_{e_1 e_2}$). The lower panels display the ratio of the normalised distributions $t\bar{t}W^+/t\bar{t}W^-$. The NLO NNPDF3.0 PDF set is employed and $\mu_R = \mu_F = H_T/3$ is used

To summarise this part, as anticipated both $t\bar{t}W^+$ and $t\bar{t}W^-$ production processes show a good level of similarity. In addition to what has already been demonstrated in Ref. [32], namely that the dominant higher order QCD effects are alike for $t\bar{t}W^+$ and $t\bar{t}W^-$, we have shown here that the kinematics (shapes of various differential cross sections) of the two processes is much the same. Such similarities are there because the differences in the PDFs for the valence quarks do not manifest themselves so much for the chosen observables. The fact that the QCD corrections are not flavour sensitive does not destroy the picture when NLO corrections in QCD are added. Furthermore, it justifies the use of correlated scales later on. For both processes, our findings are not modified when the fixed scale choice $\mu_R = \mu_F = \mu_0 = m_t + m_W/2$ is used instead or when different PDF sets are employed. We further note that, the ratio is built of integrated cross section and the peak region is very similar in both distributions. One could still point out that the normalisation matters. On the

other hand, the normalization is driven by the same power of α_s in both processes, which necessarily cancels. Hence, it matters very much that the NLO corrections may be calculated with correlated scales.

Finally, in the appendix A we review the Kolmogorov–Smirnov (KS) test, that may be used to provide a quantitative measure of similarity between two given processes. Not only do we argue there for the usefulness of the KS test at great length but we also discuss its shortcomings and advantages. This novel approach is not used as a theoretical argument for the correlation of the tested processes. It is rather an interesting way of showing that two processes are similar in various differential distributions. Thus, used alone the KS test is not a sufficient argument to prove the correlation between $t\bar{t}W^+$ and $t\bar{t}W^-$. However, used together with all other arguments mentioned in this section it increases the confidence that $t\bar{t}W^+$ and $t\bar{t}W^-$ are indeed very similar.
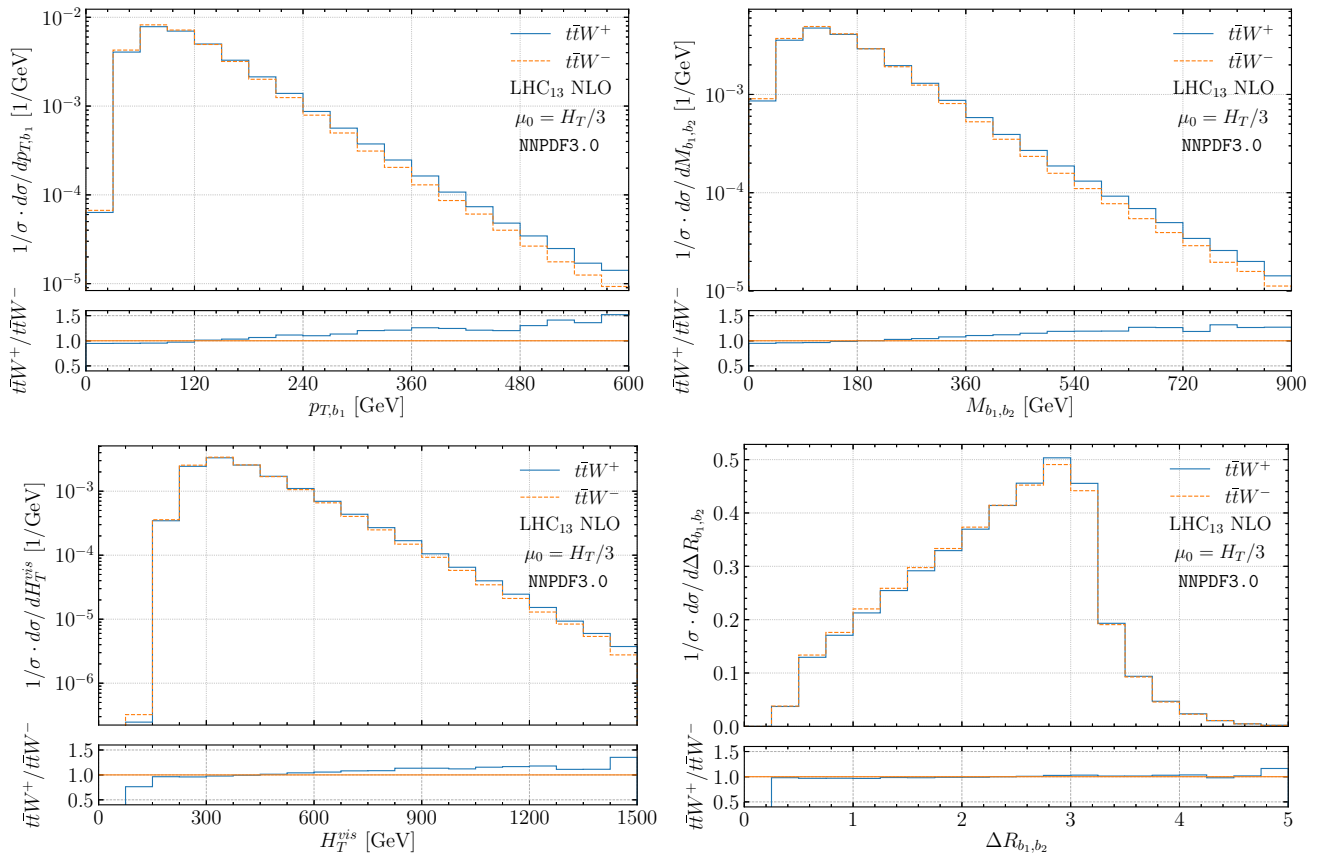
Fig. 2 As in Fig. 1 but for the transverse momentum of the hardest b-jet (p_{T,b_1}), the invariant mass of the two b-jets ($M_{b_1 b_2}$), the scalar sum of the transverse momenta of the visible final states (H_T^{vis}) and the distance in the azimuthal angle rapidity plane between the two b-jets ($\Delta R_{b_1 b_2}$)

4 Cross section ratios

Once we established that $pp \rightarrow t\bar{t}W^+$ and $t\bar{t}W^-$ are correlated we can look at their ratio with the goal of increasing the precision of NLO QCD predictions for both processes. We take the ratio of $t\bar{t}W^+$ and $t\bar{t}W^-$ at the next-to-leading order in QCD. We do not concentrate on $\mathcal{R} = \sigma_{t\bar{t}W^+}^{\text{LO}}/\sigma_{t\bar{t}W^-}^{\text{LO}}$, as in the lowest order in perturbation expansion the dependence on the strong coupling constant cancels out completely resulting in highly underestimated theoretical uncertainties for the cross section ratio. Consequently, the NLO in QCD is the first order where the theoretical uncertainties are meaningful for the $\mathcal{R}$ observable. Indeed, for the fixed scale choice, $\mu_0 = m_t + m_W/2$, we have

$$\sigma_{t\bar{t}W^+}^{\text{LO}} = 106.88^{+27.75\,(26\%)\ +4.45\,(4\%)}_{-20.53\,(19\%)\ -4.45\,(4\%)}\ [\text{ab}],$$
$$\sigma_{t\bar{t}W^-}^{\text{LO}} = 57.24^{+14.92\,(26\%)\ +2.79\,(5\%)}_{-11.04\,(19\%)\ -2.79\,(5\%)}\ [\text{ab}]. \qquad (7)$$

The first sub- and super-scripts indicate the scale variation while the second ones the PDF uncertainties. The LO cross section ratio reads

$$\mathcal{R} = \sigma_{t\bar{t}W^+}^{\text{LO}}/\sigma_{t\bar{t}W^-}^{\text{LO}} = 1.867^{+0.002\,(\ 0.1\%)\ +0.057\,(3\%)}_{-0.001\,(0.05\%)\ -0.057\,(3\%)}. \qquad (8)$$

Thus, the scale dependence is at the 0.1% level. The NLO QCD corrections to $\mathcal{R}$ are negative and of the order of 3%. Consequently, the LO scale uncertainties underestimate the size of the NLO corrections by a factor of 30. Similar behaviour is observed for the dynamical scale setting. Specifically, for $\mu_0 = H_T/3$ we obtain

$$\sigma_{t\bar{t}W^+}^{\text{LO}} = 115.10^{+30.50\,(26\%)\ +4.80\,(4\%)}_{-22.45\,(20\%)\ -4.80\,(4\%)}\ [\text{ab}],$$
$$\sigma_{t\bar{t}W^-}^{\text{LO}} = 62.40^{+16.67\,(27\%)\ +3.05\,(5\%)}_{-12.27\,(20\%)\ -3.05\,(5\%)}\ [\text{ab}]. \qquad (9)$$

The LO cross section ratio for the dynamical scale setting yields

$$\mathcal{R} = \sigma_{t\bar{t}W^+}^{\text{LO}}/\sigma_{t\bar{t}W^-}^{\text{LO}} = 1.844^{+0.004\,(0.2\%)\ +0.056\,(3\%)}_{-0.003\,(0.2\%)\ -0.056\,(3\%)}. \qquad (10)$$

In this case the NLO QCD corrections to $\mathcal{R}$ are also negative but slightly smaller at only 2%.

We choose the renormalisation and factorisation scales in the numerator and denominator in a correlated way and we always choose the same values for the scales in both the numerator and the denominator. This approach is justified by the outcomes of the previous section, i.e. by observing that various NLO distributions for $t\bar{t}W^+$ and $t\bar{t}W^-$ have

very similar shapes. In other words, the ratio $\mathcal{R}$ is rather constant across the dominant parts of phase space. This form of kinematic correlation indicates that NLO predictions for the two processes are dominated by the same topologies.

In Tables 1 and 2 we present integrated fiducial cross sections at NLO in QCD for $pp \to t\bar{t}W^+$ and $t\bar{t}W^-$ in the multi-lepton decay channel together with the theoretical uncertainties due to scale dependence for $\mu_F = \mu_R = \mu_0$ where $\mu_0 = m_t + m_W/2$ or $\mu_0 = H_T/3$. The uncertainty on higher orders for the integrated fiducial cross sections is estimated by varying μ_R and μ_F independently around a central scale μ_0 in the range $1/2 \le \mu_R/\mu_0, \mu_F/\mu_0 \le 2$ with the additional condition $1/2 \le \mu_R/\mu_F \le 2$. As it is always done we search for the minimum and maximum of the resulting cross sections. For the PDF error we use the corresponding prescription from the NNPDF3.0 group to provide the 68% confidence level (C.L.) PDF uncertainties. Specifically, the NNPDF3.0 group uses the Monte Carlo sampling method in conjunction with neural networks and the PDF uncertainties are obtained with the help of the replicas method, see e.g. [71]. Also given in Tables 1 and 2 is the $\mathcal{R}$ cross section ratio and its systematic uncertainties δ_{scale} and δ_{PDF}. To properly account for the cross-correlations between the two processes the latter is evaluated in the similar fashion as δ_{PDF} for $\sigma^{\text{NLO}}_{t\bar{t}W^+}$ and $\sigma^{\text{NLO}}_{t\bar{t}W^-}$. First we examine the stability of $\mathcal{R}$ with respect to the $p_{T,b}$ cut. To this end, we show results for four different values of the $p_{T,b}$ cut. We observe very stable cross section ratio results both in terms of the central value and theoretical uncertainties. Furthermore, we notice that the scale choice does not play any role for such an inclusive observable. The PDF uncertainties, which for $pp \to t\bar{t}W^+$ and $pp \to t\bar{t}W^-$ are consistently at the 2% level, do not cancel out substantially in the cross section ratio. The final theoretical error receives similar contributions from δ_{scale} and δ_{PDF}. These uncertainties are both at the 2% level. Such precise theoretical predictions have normally been obtained only once the NNLO QCD corrections are incorporated. Thus, $\mathcal{R}$ at NLO in QCD represents a very precise observable to be measured at the LHC. A few comments are in order here. NLO correlations for $t\bar{t}W^+$ and $t\bar{t}W^-$ are completely insensitive to potentially large gg-induced NNLO corrections to the $\mathcal{R} = \sigma^{\text{NLO}}_{t\bar{t}W^+}/\sigma^{\text{NLO}}_{t\bar{t}W^-}$ ratio. For example, due to the fact that the gg initial state is the same for the two processes we can assume that the $t\bar{t}W^+$ and $t\bar{t}W^-$ cross sections receive the same gg-channel correction, which we denote as $\delta\sigma^{\text{NNLO}}_{gg}$. As a result, the ratio would be shifted by a relative factor $\delta\mathcal{R}/\mathcal{R} \approx (\mathcal{R} - 1)\delta\sigma^{\text{NNLO}}_{gg}/\sigma^{\text{NLO}}_{t\bar{t}W^+} \approx \delta\sigma^{\text{NNLO}}_{gg}/\sigma^{\text{NLO}}_{t\bar{t}W^+}$, which could in principle amount to several percent. Therefore, it could be well above the reported uncertainty estimate of $1\% - 2\%$. The judgment of the scale variation prescription for $\mathcal{R}$ would of course be much easier in the presence of NNLO QCD calculations. Unfortunately such

calculations are out of reach even for the simplest case of $pp \to t\bar{t}W^{\pm}$ production with stable top quarks and $W^{\pm}$ gauge bosons. Adding decays of the unstable particles and incorporating the complete off-shell effects is simply difficult to imagine at the current stage of NNLO QCD calculations. Nevertheless, in the absence of the NNLO calculations for the process at hand we can assess the gg-channel correction $\delta\sigma^{\text{NNLO}}_{gg}$ by performing a LO study for $gg \to e^+\nu_e\,\mu^-\bar{\nu}_\mu\,e^+\nu_e\,b\bar{b}\,\bar{u}d$ and $gg \to e^+\nu_e\,\mu^-\bar{\nu}_\mu\,e^+\nu_e\,b\bar{b}\,\bar{c}s$ with the same input parameters, cuts and for example by employing the fixed scale choice. The size of $\delta\sigma^{\text{NNLO}}_{gg}/\sigma^{\text{NLO}}_{t\bar{t}W^+}$ correction estimated in this way amounts to 0.3%. Similar studies can be performed for $gg \to e^-\bar{\nu}_e\,\mu^+\nu_\mu\,e^-\bar{\nu}_e\,b\bar{b}\,u\bar{d}$ and $gg \to e^-\bar{\nu}_e\,\mu^+\nu_\mu\,e^-\bar{\nu}_e\,b\bar{b}\,c\bar{s}$. To evaluate LO cross sections, however, we have used cuts on light jets that are not there when the true NNLO QCD corrections are calculated. To remedy this in the next step we have used the SecToR Improved Phase sPacE for real Radiation (STRIPPER) library [78–81] that implements a general subtraction scheme for the evaluation of NNLO QCD contributions from double-real radiation to processes with at least two particles in the final state at LO. By employing STRIPPER[1] we were able to calculate the actual contribution $\delta\sigma^{\text{NNLO}}_{gg}/\sigma^{\text{NLO}}_{t\bar{t}W^+}$ for the $pp \to t\bar{t}W^+$ process with stable top quarks and W^+ gauge boson. This contribution is of the order of 0.2%, thus, it is similar in size to $\delta\sigma^{\text{NNLO}}_{gg}/\sigma^{\text{NLO}}_{t\bar{t}W^+}$ estimated by the LO studies with the complete top quark and $W^{\pm}$ off-shell effects included. Notably, it is also well below the reported uncertainty estimate for the $\mathcal{R} = \sigma^{\text{NLO}}_{t\bar{t}W^+}/\sigma^{\text{NLO}}_{t\bar{t}W^-}$ ratio (1% − 2%). Because of that, the impact of the gg-channel on the ratio at hand is quite small.

We note here, that there are different approaches in the literature for handling of uncertainties in ratios. For example one can take the relative size of the last considered order compared to the previous one as an estimate of the perturbative uncertainty, see e.g. Ref. [82]. Specifically, following [82] one can define

$$\delta_{pert.} = \pm \left| 1 - \frac{\mathcal{R}^{\text{NLO}}(\mu_0)}{\mathcal{R}^{\text{LO}}(\mu_0)} \right| \times 100\%, \qquad (11)$$

where the values of μ_0 are chosen in a correlated way in the numerator and the denominator of $\mathcal{R}$. This error estimator assumes that the sub-leading terms should be smaller than the last known correction. The obvious downside to this approach is that it gives a vanishing result whenever two consecutive perturbative orders provide identical numerical predictions. Furthermore, this prescription leads to the rather suspicious shapes of the uncertainty bands for the differential cross section ratios. Thus, as clearly stated in Ref. [82] this approach on its own can not serve as a good estimator of per-

---

[1] Courtesy of M. Czakon.

Table 1 NLO QCD integrated fiducial cross sections for $pp \to t\bar{t}W^{\pm}$ in the multi-lepton final state at the LHC with $\sqrt{s} = 13$ TeV. Also shown are results for $\mathcal{R} = \sigma_{t\bar{t}W^+}^{\mathrm{NLO}}/\sigma_{t\bar{t}W^-}^{\mathrm{NLO}}$. Theoretical uncertainties as estimated from the scale variation and from the PDFs are listed as well. Four different values of the $p_{T,b}$ cut are used. The NNPDF3.0 PDF set is employed and $\mu_R = \mu_F = \mu_0$ where $\mu_0 = m_t + m_W/2$

$\mu_0 = m_t + m_W/2$ NNPDF3.0	$\sigma_{t\bar{t}W^+}^{\mathrm{NLO}} \pm \delta_{\mathrm{scale}} \pm \delta_{\mathrm{PDF}}$ [ab]	$\sigma_{t\bar{t}W^-}^{\mathrm{NLO}} \pm \delta_{\mathrm{scale}} \pm \delta_{\mathrm{PDF}}$ [ab]	$\mathcal{R} \pm \delta_{\mathrm{scale}} \pm \delta_{\mathrm{PDF}}$ $\mathcal{R} = \sigma_{t\bar{t}W^+}^{\mathrm{NLO}}/\sigma_{t\bar{t}W^-}^{\mathrm{NLO}}$
$p_{T,b} > 25$ GeV	$123.2^{+6.3\,(5\%)\,+2.1\,(2\%)}_{-8.7\,(7\%)\,-2.1\,(2\%)}$	$68.0^{+4.8\,(7\%)\,+1.2\,(2\%)}_{-5.5\,(8\%)\,-1.2\,(2\%)}$	$1.81^{+0.02\,(1\%)\,+0.03\,(2\%)}_{-0.03\,(2\%)\,-0.03\,(2\%)}$
$p_{T,b} > 30$ GeV	$113.1^{+5.4\,(5\%)\,+1.9\,(2\%)}_{-7.8\,(7\%)\,-1.9\,(2\%)}$	$62.3^{+4.2\,(7\%)\,+1.1\,(2\%)}_{-4.9\,(8\%)\,-1.1\,(2\%)}$	$1.81^{+0.02\,(1\%)\,+0.03\,(2\%)}_{-0.04\,(2\%)\,-0.03\,(2\%)}$
$p_{T,b} > 35$ GeV	$102.6^{+4.7\,(5\%)\,+1.7\,(2\%)}_{-6.8\,(7\%)\,-1.7\,(2\%)}$	$56.3^{+3.7\,(7\%)\,+1.0\,(2\%)}_{-4.4\,(8\%)\,-1.0\,(2\%)}$	$1.82^{+0.02\,(1\%)\,+0.03\,(2\%)}_{-0.04\,(2\%)\,-0.03\,(2\%)}$
$p_{T,b} > 40$ GeV	$92.0^{+4.0\,(4\%)\,+1.6\,(2\%)}_{-6.1\,(7\%)\,-1.6\,(2\%)}$	$50.3^{+3.3\,(6\%)\,+0.9\,(2\%)}_{-3.9\,(8\%)\,-0.9\,(2\%)}$	$1.83^{+0.02\,(1\%)\,+0.03\,(2\%)}_{-0.04\,(2\%)\,-0.03\,(2\%)}$

Table 2 As in Table 1 but for $\mu_0 = H_T/3$

$\mu_0 = H_T/3$ NNPDF3.0	$\sigma_{t\bar{t}W^+}^{\mathrm{NLO}} \pm \delta_{\mathrm{scale}} \pm \delta_{\mathrm{PDF}}$ [ab]	$\sigma_{t\bar{t}W^-}^{\mathrm{NLO}} \pm \delta_{\mathrm{scale}} \pm \delta_{\mathrm{PDF}}$ [ab]	$\mathcal{R} \pm \delta_{\mathrm{scale}} \pm \delta_{\mathrm{PDF}}$ $\mathcal{R} = \sigma_{t\bar{t}W^+}^{\mathrm{NLO}}/\sigma_{t\bar{t}W^-}^{\mathrm{NLO}}$
$p_{T,b} > 25$ GeV	$124.4^{+4.3\,(3\%)\,+2.1\,(2\%)}_{-7.7\,(6\%)\,-2.1\,(2\%)}$	$68.6^{+3.5\,(5\%)\,+1.2\,(2\%)}_{-4.8\,(7\%)\,-1.2\,(2\%)}$	$1.81^{+0.02\,(1\%)\,+0.03\,(2\%)}_{-0.03\,(2\%)\,-0.03\,(2\%)}$
$p_{T,b} > 30$ GeV	$113.9^{+3.5\,(3\%)\,+1.9\,(2\%)}_{-6.8\,(6\%)\,-1.9\,(2\%)}$	$62.7^{+3.0\,(5\%)\,+1.1\,(2\%)}_{-4.3\,(7\%)\,-1.1\,(2\%)}$	$1.82^{+0.02\,(1\%)\,+0.03\,(2\%)}_{-0.03\,(2\%)\,-0.03\,(2\%)}$
$p_{T,b} > 35$ GeV	$103.1^{+3.1\,(3\%)\,+1.7\,(2\%)}_{-6.0\,(6\%)\,-1.7\,(2\%)}$	$56.5^{+2.6\,(5\%)\,+1.0\,(2\%)}_{-3.8\,(7\%)\,-1.0\,(2\%)}$	$1.82^{+0.02\,(1\%)\,+0.03\,(2\%)}_{-0.03\,(2\%)\,-0.03\,(2\%)}$
$p_{T,b} > 40$ GeV	$92.3^{+2.8\,(3\%)\,+1.5\,(2\%)}_{-5.3\,(6\%)\,-1.5\,(2\%)}$	$50.4^{+2.3\,(5\%)\,+0.9\,(2\%)}_{-3.4\,(7\%)\,-0.9\,(2\%)}$	$1.83^{+0.02\,(1\%)\,+0.03\,(2\%)}_{-0.03\,(2\%)\,-0.03\,(2\%)}$

turbative uncertainties. Nevertheless, it can be used in conjunction with traditional methods to further ensure that the correlated scale dependence is indeed a reasonable approach. Had we used the prescription from Eq. (11) we would obtain $\delta_{pert.} = 3\%$ for $\mu_0 = m_t + m_W/2$ and $\delta_{pert.} = 2\%$ for the dynamical scale setting. Thus, the uncertainty estimate for the $\mathcal{R} = \sigma_{t\bar{t}W^+}^{\mathrm{NLO}}/\sigma_{t\bar{t}W^-}^{\mathrm{NLO}}$ ratio would rather be $\delta_{pert.} = 2\% - 3\%$, which is only slightly larger than $\delta_{\mathrm{scale}} = 1\% - 2\%$.

In the next step we examine the impact of the top quark production and decay modelling on the cross section ratio. To this end we present results for the full NWA and for the NWA$_{\mathrm{LOdecay}}$ case. The former comprises NLO QCD corrections to the production and to the subsequent top quark decays, the latter NLO QCD corrections to the production of $t\bar{t}W^{\pm}$ and LO top quark decays. Should we use the NLO QCD results in the full NWA for the $pp \to t\bar{t}W^{\pm}$ process our findings for $\mu_0 = m_t + m_W/2$ would be as follows

$$\mathcal{R} = \frac{\sigma_{t\bar{t}W^+}^{\mathrm{NLO,\,NWA}}}{\sigma_{t\bar{t}W^-}^{\mathrm{NLO,\,NWA}}} = 1.81 \pm 0.04\,(2\%)\,, \qquad (12)$$

where the quoted theoretical error results only from the scale dependence as the PDF uncertainties will not be affected by changes in the modeling of the top quark decays. On the other hand for the dynamical scale choice $\mu_0 = H_T/3$ we would obtain

$$\mathcal{R} = \frac{\sigma_{t\bar{t}W^+}^{\mathrm{NLO,\,NWA}}}{\sigma_{t\bar{t}W^-}^{\mathrm{NLO,\,NWA}}} = 1.81 \pm 0.03\,(2\%)\,. \qquad (13)$$

We can observe that the full NWA approach does not modify either the value or the size of the theoretical error for the integrated cross section ratio. The latter result is not surprising taking into account that the impact of the top quark off-shell effects on the integrated fiducial $t\bar{t}W^{\pm}$ cross section is negligible. Furthermore, theoretical uncertainties for the full NWA and full off-shell case are similar independently of the scale choice [32].

Finally, we have employed the NWA$_{\mathrm{LOdecay}}$ case. For $\mu_0 = m_t + m_W/2$ we obtained

$$\mathcal{R} = \frac{\sigma_{t\bar{t}W^+}^{\mathrm{NLO,\,NWA_{LOdecay}}}}{\sigma_{t\bar{t}W^-}^{\mathrm{NLO,\,NWA_{LOdecay}}}} = 1.82 \pm 0.02\,(1\%)\,, \qquad (14)$$

whereas for $\mu_0 = H_T/3$ we can report

$$\mathcal{R} = \frac{\sigma_{t\bar{t}W^+}^{\mathrm{NLO,\,NWA_{LOdecay}}}}{\sigma_{t\bar{t}W^-}^{\mathrm{NLO,\,NWA_{LOdecay}}}} = 1.81 \pm 0.02\,(1\%)\,. \qquad (15)$$

Even for this case the cross section ratios are very stable and rather insensitive to the details of the modelling of the top quark production and decays. Let us note here, that for the absolute $pp \to t\bar{t}W^{\pm}$ integrated cross sections the difference between the NWA$_{\mathrm{LOdecay}}$ approach and the full off-shell one is at the level of 5%. In addition, theoretical uncertainties due to the scale dependence are higher in the former case, up to 11–13% [32]. Yet in the cross section ratio these differences cancel out making $\mathcal{R} = \sigma_{t\bar{t}W^+}^{\mathrm{NLO}}/\sigma_{t\bar{t}W^-}^{\mathrm{NLO}}$ very pre-

cise and an extremely interesting theoretical observable to be measured at the LHC.

To conclude this part, we note that for the cross section ratio at NLO in QCD the residual perturbative uncertainties are reduced to $1\% - 2\%$ and are similar in size to the PDF uncertainties. The theoretical uncertainties associated with the top quark decay modelling are negligible. This suggests that the $\mathcal{R} = \sigma_{t\bar{t}W^+}^{\mathrm{NLO}}/\sigma_{t\bar{t}W^-}^{\mathrm{NLO}}$ observable can be employed either for the precision SM measurements or to shed some light on possible new physics scenarios that might reveal themselves only once sufficiently precise theoretical predictions are available. For example in the case of BSM physics the presence of two same-sign leptons in the final state, a relatively rare phenomenon at the LHC, constitutes an optimal signature for many new physics models from supersymmetry, supergravity and Majorana neutrinos to models with the modified Higgs boson sector. Given the final accuracy of $\mathcal{R}$, it should be used to put more stringent constrains on the parameter space of these models.

5 Charge asymmetries in $t\bar{t}W^{\pm}$ production

The pp initial state at the LHC is expected to produce top quark and antiquark rapidity distributions that are symmetric about $y = 0$ in $t\bar{t}$ production. However, since the quarks in the initial state can be from valence quarks, while the antiquarks are from the sea, the larger average momentum-fraction of quarks leads to an excess of top quarks produced in the forward directions. The rapidity distribution of top quarks in the SM is therefore broader than that of the more centrally produced top antiquarks. This suggests that $\Delta|y| = |y_t| - |y_{\bar{t}}|$, which is the difference between the absolute value of the top quark rapidity $|y_t|$ and the absolute value of the anti-top quark rapidity $|y_{\bar{t}}|$, is a suitable observable to measure the top quark charge asymmetry at the LHC. This asymmetry is nevertheless very small, see e.g. [83,84]. For the $pp \to t\bar{t}W^{\pm}$ process the presence of the $W^{\pm}$ gauge boson results in the top quark charge asymmetry that is significantly larger than in $t\bar{t}$ production [7]. The main reason behind this is the absence of the symmetric gg channel that is not accessible until NNLO. Furthermore, the emission of the $W^{\pm}$ gauge boson from the initial state polarises the initial quark line and in turn the $t\bar{t}$ pair. As a result, the charge asymmetries for the top quark decay products are large and already present at the leading order. In the following we calculate afresh the top quark charge asymmetry in the $t\bar{t}W^{\pm}$ process in the multi-lepton final state using the state-of-the-art NLO QCD calculations with the full top quark off-shell effects included. Additionally, the asymmetries for the top quark decay products, A_c^b and A_c^ℓ, will be examined. In this part of the paper, one of our main goals is to carefully assess the impact of the top quark modelling on A_c^t, A_c^b and A_c^ℓ. We start with asymmetries at the inte-

grated level albeit in the fiducial regions of the phase space as defined in Sect. 2. For A_c^ℓ we will additionally calculate the differential and cumulative asymmetry with respect to the following observables: $p_T(\ell_t\ell_{\bar{t}})$, $|y(\ell_t\ell_{\bar{t}})|$ and $M(\ell_t\ell_{\bar{t}})$, where ℓ_t, $\ell_{\bar{t}}$ stands for the charged leptons stemming from the top and anti-top quark decay respectively. For the two processes under consideration $pp \to e^+\nu_e \mu^-\bar{\nu}_\mu e^+\nu_e b\bar{b}$ and $pp \to e^-\bar{\nu}_e \mu^+\nu_\mu e^-\bar{\nu}_e b\bar{b}$ the reconstruction of the (anti-)top quark momentum through its decay products is required. As we are dealing with identical leptons in the final state, however, we must employ an additional mechanism to properly assign the positron (electron) and the corresponding neutrino ν_e (anti-neutrino $\bar{\nu}_e$) to the correct top (anti-top) quark. In the case of $t\bar{t}W^+$ production we use the following four different resonance histories (a similar procedure is applied in the $t\bar{t}W^-$ case)

$$
\begin{aligned}
t &\to e_1^+ \nu_{e,1} b & \text{and} & & \bar{t} &\to \mu^- \bar{\nu}_\mu \bar{b}, \\
t &\to e_1^+ \nu_{e,2} b & \text{and} & & \bar{t} &\to \mu^- \bar{\nu}_\mu \bar{b}, \\
t &\to e_2^+ \nu_{e,1} b & \text{and} & & \bar{t} &\to \mu^- \bar{\nu}_\mu \bar{b}, \\
t &\to e_2^+ \nu_{e,2} b & \text{and} & & \bar{t} &\to \mu^- \bar{\nu}_\mu \bar{b}.
\end{aligned}
\tag{16}
$$

These four resonant histories are not sufficient if NLO QCD calculations are considered. In the case of the subtracted real emission part we additionally take into account the extra light jet if resolved. Specifically, to closely mimic what is done on the experimental side only the light jet that passes all the cuts, that are also required for the two b-jets, is added to the resonance history. Thus, in such a case a total of twelve different resonant histories have to be considered. We compute for each history the following quantity, see Ref. [85]

$$
\mathcal{Q} = |M_t - m_t| + |M_{\bar{t}} - m_t|,
\tag{17}
$$

where M_t and $M_{\bar{t}}$ are the (reconstructed) invariant masses of the top and anti-top quark respectively and $m_t = 172.5$ GeV. For each phase space point we pick the history that minimises the $\mathcal{Q}$ value. In this way all the (anti-)top quark decay products are identified. They are employed in the definition of A_c^t, A_c^ℓ and A_c^b. To show how well such a reconstruction works in Fig. 3 we display the reconstructed invariant mass of the top (anti-top) quark at NLO in QCD for the $pp \to t\bar{t}W^+$ ($pp \to t\bar{t}W^-$) process in the multi-lepton channel. Out of all twelve histories the four histories with the smallest $\mathcal{Q}$ value are shown. Clearly one can see that the reconstruction works very well.

Using the notation of Refs. [84,86,87] we define the top quark charge asymmetry as follows

$$
A_c^t = \frac{\sigma_{\mathrm{bin}}^+ - \sigma_{\mathrm{bin}}^-}{\sigma_{\mathrm{bin}}^+ + \sigma_{\mathrm{bin}}^-}, \quad \sigma_{\mathrm{bin}}^{\pm} = \int \theta(\pm\Delta|y|)\,\theta_{\mathrm{bin}}\,d\sigma,
\tag{18}
$$

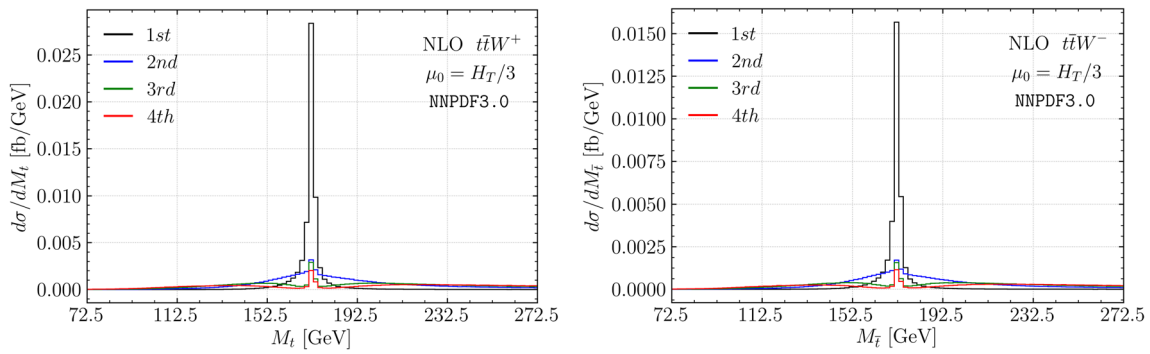**Fig. 3** Reconstructed invariant mass of the top quark and anti-top quark at NLO in QCD for $pp \to t\bar{t}W^+$ and $pp \to t\bar{t}W^-$ in the multi-lepton final state. Results are given for the LHC with $\sqrt{s} = 13$ TeV. The NLO NNPDF3.0 PDF set is employed and $\mu_R = \mu_F = \mu_0$ where $\mu_0 = H_T/3$

where $\Delta|y| = |y_t| - |y_{\bar{t}}|$ and $d\sigma$ is the differential fiducial $t\bar{t}W^\pm$ cross section calculated at NLO in QCD. The binning function θ_{bin} can take the values zero or one. Its purpose is to restrict to a given bin the kinematics of the $t\bar{t}W^\pm$ process in one of the kinematic variables that is considered. The integrated asymmetry is obtained by setting $\theta_{\text{bin}} = 1$. We note here that the charge-symmetric gg initial state, that is the dominant mechanism for $t\bar{t}$ production at the LHC, is not present for $t\bar{t}W^\pm$ production. Therefore, unlike for $pp \to t\bar{t}$, it will not contribute to the denominator of Eq. (18) to dilute the asymmetry. The LHC measurements for the top quark charge asymmetry in $pp \to t\bar{t}$ production have been carried out in terms of rapidity as well as pseudorapidity differences, see e.g. [88–93]. Even-though, the top quark charge asymmetry based on rapidity and pseudorapidity has the same features its value can differ quite substantially. Consequently, we shall provide results for A_c^t for both cases. In the case of the top quark decay products A_c^ℓ and A_c^b are based on $\Delta|y| = |y_{\ell_t}| - |y_{\ell_{\bar{t}}}|$ and $\Delta|y| = |y_b| - |y_{\bar{b}}|$ respectively.

The top quark charge asymmetry can be visualised by superimposing the rapidity (or the pseudo-rapidity) of t and $\bar{t}$ for the $t\bar{t}W^+$ process. The same can be done separately for $t\bar{t}W^-$. Similarly, we can plot together the top and anti-top quark decay products, b and $\bar{b}$ as well as ℓ_t and $\ell_{\bar{t}}$. In Fig. 4 we present such a comparison at the NLO QCD level for the $t\bar{t}W^\pm$ process. We can observe that all spectra are symmetric about $y = 0$ ($\eta = 0$), as it should be, and that the anti-top quark is more central with respect to the top quark. The same is visible for the b-jet. This can be directly translated into the positive value of A_c^t and A_c^b. The situation is reversed for the charged leptons. In the later case the charged lepton from the top quark decay is more central, which will manifest itself in the negative value of A_c^ℓ.

In Tables 3 and 4 we present our findings for A_c^t, A_c^ℓ and A_c^b at NLO QCD for $t\bar{t}W^+$ production in the multi-lepton channel at the LHC with $\sqrt{s} = 13$ TeV. Results are given for the fixed scale choice $\mu_R = \mu_F = m_t + m_W/2$. The top quark charge asymmetry calculated in terms of rapidities (pseudo-

rapidities) is denoted as $A_{c,y}^t$ ($A_{c,\eta}^t$). We present the results with the full off-shell effects included as well as for the full NWA and for the NWA$_{\text{LOdecay}}$ case. For all three approaches theoretical uncertainties due to the scale dependence are also given. They are estimated by varying the renormalisation and factorisation scales in α_s and PDFs up and down by a factor of 2 around the central scale of the process μ_0. We show theoretical predictions for the unexpanded and expanded version of the asymmetry. As the ratio in Eq. (18) generates contributions of $\mathcal{O}(\alpha_s^2)$ and higher, which in principle can be affected by the unknown NNLO contributions, we expand A_c^i to first order in α_s. The expanded version of A_c^i at NLO in QCD, where i stands for $i = t, \ell, b$, is defined as

$$A_{c,exp}^i = \frac{\sigma_{\text{LO}}^-}{\sigma_{\text{LO}}^+} \left(1 + \frac{\delta\sigma_{\text{NLO}}^-}{\sigma_{\text{LO}}^-} - \frac{\delta\sigma_{\text{NLO}}^+}{\sigma_{\text{LO}}^+} \right). \tag{19}$$

where $\sigma^\pm$ stands for $\sigma^\pm = \sigma_{\text{bin}}^+ \pm \sigma_{\text{bin}}^-$ and $\delta\sigma_{\text{NLO}}^\pm$ are the NLO contributions to the fiducial cross section. Furthermore, $\sigma_{\text{LO}}^\pm$ are evaluated with NLO input parameters. In Tables 3 and 4 we include in parenthesis the Monte Carlo (MC) integration errors to show that the latter are smaller than or at least similar in size to the theoretical errors from the scale dependence. Since the PDF dependence of the asymmetry is very small (at the per-mill level) we do not quote the PDF errors in our predictions.

Before we analyse our results we remind the reader that the results presented in Ref. [7] were generated for NLO+PS and for a different setup and input parameters. Thus, a direct comparison for the absolute values for $A_{c,\eta}^t$, $A_{c,y}^b$, $A_{c,y}^\ell$ is not possible, but we are rather interested in the relative size of their theoretical uncertainties. In Ref. [7] LO spin correlations are incorporated with the help of MADSPIN. The latter is employed before events can be passed to HERWIG6 [94]. The two charged leptons coming from top and anti-top quark decays are chosen to be respectively positrons and electrons, while the extra $W^\pm$ bosons decay into muons. Consequently, leptons and b-jets coming from the top and anti-top
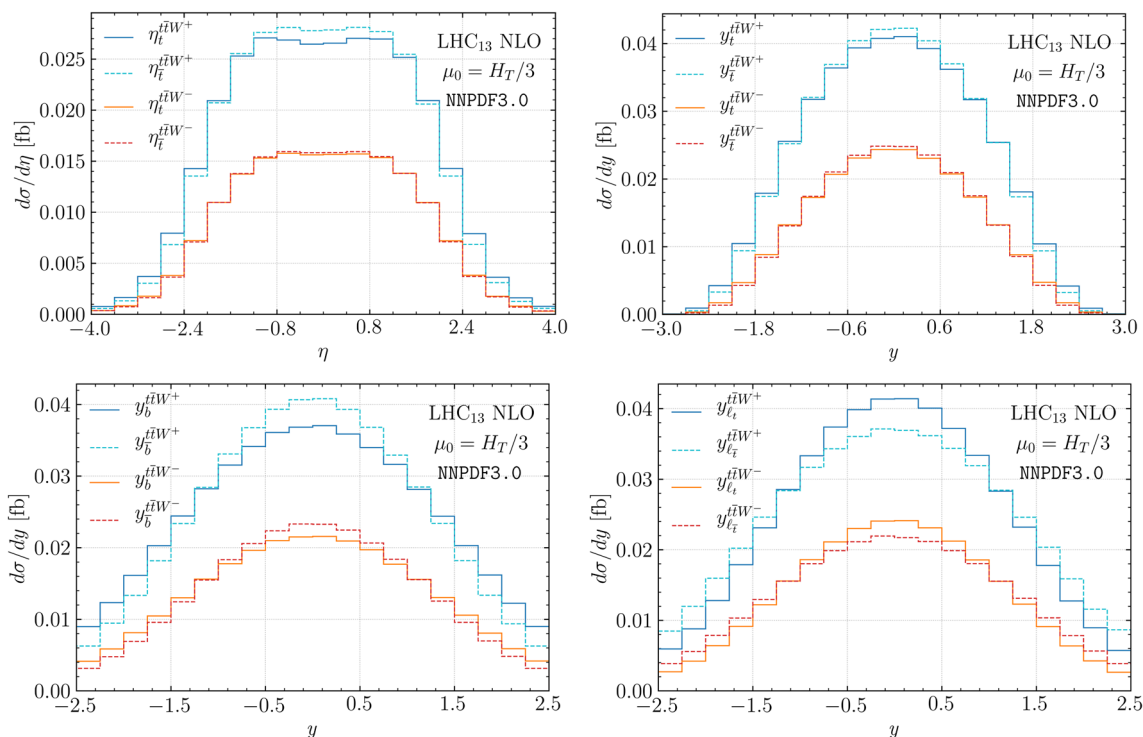
Fig. 4 Comparison of the rapidity and pseudo-rapidity distributions of the t and $\bar{t}$ quarks at the NLO QCD level for $pp \rightarrow t\bar{t}W^+$ and $pp \rightarrow t\bar{t}W^-$ in the multi-lepton final state. Also shown are rapid-ity distributions of the charged leptons and b-jets from t and $\bar{t}$ decays. Results are given for the LHC with $\sqrt{s} = 13$ TeV. The NLO NNPDF3.0 PDF set is employed and $\mu_R = \mu_F = \mu_0$ where $\mu_0 = H_T/3$ is used

quark decays can be uniquely identified. Issues related to the top quark reconstruction are, therefore, not considered. The results given in Ref. [7] will serve us as a guideline in the study of the impact of the top quark reconstruction. In particular for $A_{c,\eta}^t$ theoretical uncertainties quoted in Ref. [7] are of the order of $\delta_{\rm scale} = {}^{+19\%}_{-14\%}$. For $A_{c,y}^b$ and $A_{c,y}^\ell$, on the other hand, they are $\delta_{\rm scale} = {}^{+2.5\%}_{-2.2\%}$ and $\delta_{\rm scale} = {}^{+8.5\%}_{-6.0\%}$ respectively. The results for $A_{c,\eta}^t$, $A_{c,y}^b$ and $A_{c,y}^t$ have been given for the combined $pp \rightarrow t\bar{t}W^\pm$ case and for $\mu_R = \mu_F = 2m_t$. Furthermore, for the computation of $A_{c,y}^b$, events that do not feature two b-jets coming from the top quark decays were discarded.

In the following we analyse our findings for A_c^t as reconstructed from the top quark decay products for $\mu_R = \mu_F = m_t + m_W/2$. They are presented in Table 3 and graphically depicted in Fig. 5. First we notice that the difference between the unexpanded NLO asymmetry (A_c^t) and the one with a consistent expansion in α_s ($A_{c,exp}^t$) expressed either in terms of rapidity ($A_{c,y}^t$) or pseudo-rapidity differences ($A_{c,\eta}^t$), is rather moderate for the full off-shell and the full NWA case. Specifically, the absolute value of A_c^t increases by 0.5–0.6% (by about 20–30% in the relative terms) when the expansion is introduced. For the NWA$_{\rm LOdecay}$ approach, on the other hand, we observe a larger increase by 1.1%. In addition, theoretical uncertainties due to the scale dependence

are substantially reduced for the expanded version of A_c^t. In that case we have estimated that the uncertainties are of the order of 15%, 18% and 24% depending on the approach used. These uncertainties are similar in size to uncertainties given in Ref. [7] for $A_{c,\eta}^t$. Therefore, the two definitions, A_c^t and $A_{c,exp}^t$, give reasonably consistent results especially in the full off-shell and full NWA case as it can be nicely visualised in Fig. 5. We can also note that the results for $A_{c,y}^t$ differ by almost 1% (by about 40% − 50% in the relative terms) from those for $A_{c,\eta}^t$. Only in the case of NWA$_{\rm LOdecay}$ is the difference smaller, i.e. 0.3% (15% − 35% in the relative terms). Finally, similar remarks apply to the charge asymmetry in $t\bar{t}W^-$ production.

A few comments are in order here. The A_c^t asymmetry in $t\bar{t}W^\pm$ production is rather small so any effect can have substantial influence on its absolute value. From Ref. [60] we already know, that the inclusion of the electroweak corrections increases the asymmetry only by a small amount, i.e. by about 0.16%. On the other hand, NNLO QCD corrections, which will stabilise the size of the theoretical uncertainties, can play a crucial role for A_c^t. Although NNLO QCD corrections to $t\bar{t}W^\pm$ production with $gg \rightarrow t\bar{t}W^\pm q\bar{q}'$ processes are completely symmetric and can contribute only to the denominator of A_c^t, they might still alter the value of A_c^t. First stud-

Table 3 Unexpanded and expanded A^t_c asymmetry at NLO in QCD for $pp \to t\bar{t}W^+$ in multi-lepton channel at the LHC with $\sqrt{s} = 13$ TeV. Various approaches for the modelling of the top quark production and decays are considered: the full off-shell case, the full NWA and the NWA$_{\text{LOdecay}}$ case. Also given are Monte Carlo (in parenthesis) integration and theoretical errors. The NNPDF3.0 PDF set is employed and $\mu_R = \mu_F = \mu_0$ where $\mu_0 = m_t + m_W/2$

$t\bar{t}W^+$ $\mu_0 = m_t + m_W/2$	OFF-SHELL	FULL NWA	NWA$_{\text{LOdecay}}$
$A^t_{c,y}$ [%]	$2.09(8)^{+1.06(51\%)}_{-0.70(33\%)}$	$1.68(4)^{+1.00(60\%)}_{-0.67(40\%)}$	$0.86(3)^{+0.66(77\%)}_{-0.43(50\%)}$
$A^t_{c,exp,y}$ [%]	$2.62(10)^{+0.39(15\%)}_{-0.34(13\%)}$	$2.19(4)^{+0.38(17\%)}_{-0.34(16\%)}$	$1.94(5)^{+0.46(24\%)}_{-0.32(16\%)}$
$A^t_{c,\eta}$ [%]	$3.10(8)^{+1.21(39\%)}_{-0.80(26\%)}$	$2.58(4)^{+1.31(51\%)}_{-0.75(29\%)}$	$1.16(4)^{+0.71(61\%)}_{-0.44(38\%)}$
$A^t_{c,exp,\eta}$ [%]	$3.70(10)^{+0.46(12\%)}_{-0.40(11\%)}$	$3.18(5)^{+0.56(18\%)}_{-0.34(11\%)}$	$2.25(5)^{+0.51(23\%)}_{-0.32(14\%)}$

Table 4 Unexpanded and expanded A^ℓ_c and A^b_c asymmetries at NLO in QCD for $pp \to t\bar{t}W^+$ in multi-lepton channel at the LHC with $\sqrt{s} = 13$ TeV. Various approaches for the modelling of the top quark production and decays are considered: the full off-shell case, the full NWA and the NWA$_{\text{LOdecay}}$ case. Also given are Monte Carlo (in parenthesis) integration and theoretical errors. The NNPDF3.0 PDF set is employed and $\mu_R = \mu_F = \mu_0$ where $\mu_0 = m_t + m_W/2$

$t\bar{t}W^+$ $\mu_0 = m_t + m_W/2$	OFF-SHELL	FULL NWA	NWA$_{\text{LOdecay}}$
$A^b_{c,y}$ [%]	$6.46(8)^{+0.05(0.8\%)}_{-0.05(0.8\%)}$	$6.18(4)^{+0.13(2.1\%)}_{-0.05(0.8\%)}$	$5.99(3)^{+0.10(1.7\%)}_{-0.01(0.2\%)}$
$A^b_{c,exp,y}$ [%]	$6.56(10)^{+0.02(0.3\%)}_{-0.07(1.1\%)}$	$6.28(4)^{+0.03(0.5\%)}_{-0.01(0.1\%)}$	$6.21(5)^{+0.06(1.0\%)}_{-0.01(0.2\%)}$
$A^\ell_{c,y}$ [%]	$-7.90(10)^{+2.15(27\%)}_{-1.39(17\%)}$	$-8.43(4)^{+2.10(25\%)}_{-1.37(16\%)}$	$-10.11(3)^{+1.36(13\%)}_{-0.95(9.4\%)}$
$A^\ell_{c,exp,y}$ [%]	$-7.00(12)^{+1.00(14\%)}_{-0.80(11\%)}$	$-7.52(4)^{+0.95(13\%)}_{-0.78(10\%)}$	$-8.23(5)^{+1.01(12\%)}_{-0.79(9.6\%)}$

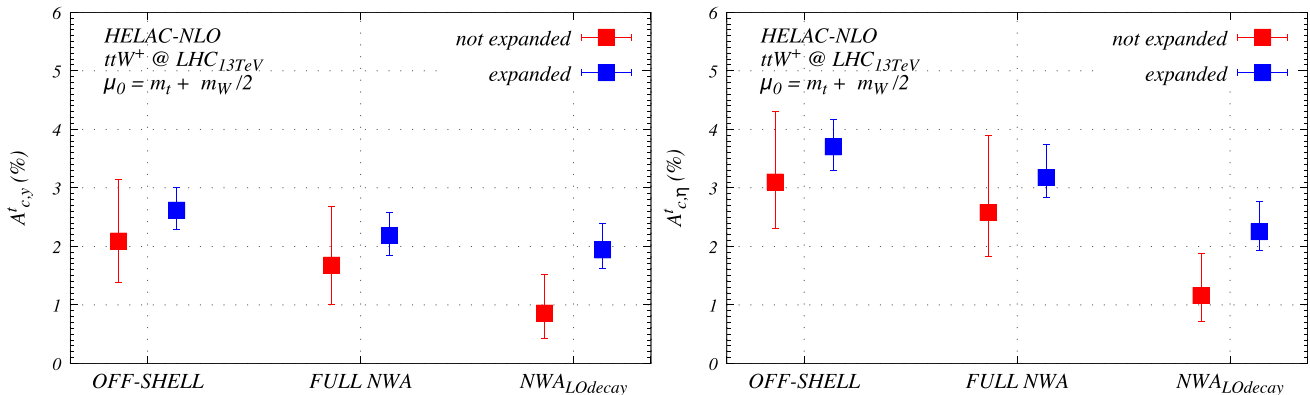**Fig. 5** Unexpanded and expanded A^t_c asymmetry at NLO in QCD for $pp \to t\bar{t}W^+$ in the multi-lepton channel at the LHC with $\sqrt{s} = 13$ TeV. Various approaches for the modelling of the top quark production and decays are considered: the full off-shell case, the full NWA and the NWA$_{\text{LOdecay}}$ case. The NNPDF3.0 PDF set is employed and $\mu_R = \mu_F = \mu_0$ where $\mu_0 = m_t + m_W/2$

ies presented in Ref. [60], with the approximate NNLO[2] to $t\bar{t}W^\pm$ where stable top quarks and $W^\pm$ gauge bosons are considered, have shown, however, that A^t_c increases by less by 0.6% and 0.8% percent for the $m(t\bar{t}W^\pm)$ and H_T based scale choices. By including these higher order effects the scale dependence is reduced to $\delta_{\text{scale}} = {}^{+6.0\%}_{-3.0\%}$ [60]. Finally,

similar effects have been observed for the $pp \to t\bar{t}$ process at the LHC for $\sqrt{s} = 8$ TeV [84] where among others the inclusive top quark charge asymmetry $A^t_{c,y}$ and $A^t_{c,exp,y}$ at NLO QCD and NNLO QCD has been studied together with NLO electroweak corrections. Even-though there is no close analogy between the higher order corrections to $t\bar{t}$ and $t\bar{t}W^\pm$ production as these processes are dominated by different partonic channels and should thus be regarded as uncorrelated/dissimilar, it is interesting to see the similar (relative) size of the various effects for $A^t_{c,y}$ and $A^t_{c,exp,y}$. The absolute

---

[2] The approximate NNLO predictions from Ref. [60] are evaluated by adding to the NLO results the $\mathcal{O}(\alpha_s^2)$ term of the expansion of the NNLL soft gluon resummation of the cross section. The soft gluon resummation concerns, however, only the Born process.

value of the top quark charge asymmetry for the $pp \rightarrow t\bar{t}$ process at the LHC is of course much smaller.

In Table 4 and in Fig. 6 we present results for the charge asymmetries of the top quark decay products A_c^{ℓ} and A_c^b for $\mu_R = \mu_F = m_t + m_W/2$. Not only are these asymmetries much larger, but the reconstruction of the top quarks is also not required. Moreover, the advantage of the A_c^{ℓ} observable in comparison to A_c^b lies in the fact that measurements of leptons are particularly precise at the LHC due to the excellent lepton energy resolution of the ATLAS and CMS detectors. For A_c^b, on the other hand, good b-jet tagging efficiency and low light jet mistag rate would be mandatory. For the full off-shell and full NWA case the difference between A_c^{ℓ} and $A_{c,exp}^{\ell}$ is 0.9% in absolute terms, thus within theoretical uncertainties of $A_{c,exp}^{\ell}$. Only in the $NWA_{LOdecay}$ case does it increase to 1.9%, which is above the theoretical scale uncertainty δ_{scale} even for A_c^{ℓ}. Overall, theoretical uncertainties for $A_{c,exp}^{\ell}$ are below 15% independently of the approach employed. Thus, they are slightly higher than in Ref. [7]. For A_c^b the situation is very stable. We observe small $0.1\% - 0.2\%$ changes between A_c^b and $A_{c,exp}^b$. Theoretical uncertainties of the order of 1% are estimated, which is similar in size to theoretical errors quoted in [7]. We can conclude this part by saying that the full NWA description is sufficient to describe A_c^t, A_c^b and A_c^{ℓ}. The inclusion of the complete off-shell effects for the $pp \rightarrow t\bar{t}W^+$ process increases the central values of the asymmetries while at the same time the theoretical errors are kept almost unchanged. We have also shown that in the case of the top quark charge asymmetry and the asymmetries of the top quark decay products the NLO QCD corrections to the top quark decays play a crucial role.

Our conclusions are not changed when the dynamical scale choice, $\mu_0 = H_T/3$, is employed instead. Results for $A_{c,}^t$, A_c^{ℓ} and A_c^b at NLO in QCD with $\mu_0 = H_T/3$ are shown in Tables 5 and 6. When comparing to the theoretical predictions for $\mu_0 = m_t + m_W/2$ we can notice an overall agreement, within $0.1\sigma - 0.7\sigma$, between all central values of the asymmetries. In addition, similar theoretical uncertainties due to the scale dependence are estimated for both scale choices.

Our state-of-the art results for the top quark charge asymmetry and for the charge asymmetries of the top quark decay products are summarised in Table 7. We provide the NLO QCD results for $A_{c,exp}^t$, $A_{c,exp}^{\ell}$ and $A_{c,exp}^b$. They are calculated from the theoretical predictions, which include the full top quark off-shell effects. We present results for $pp \rightarrow t\bar{t}W^+$ and $pp \rightarrow t\bar{t}W^-$ in the multi-lepton channel at the LHC with $\sqrt{s} = 13$ TeV. We additionally present the combined results for the $pp \rightarrow t\bar{t}W^{\pm}$ process. Also in this case the results for the top quark charge asymmetry are given in terms of rapidities, $\Delta|y| = |y_t| - |y_{\bar{t}}|$, and pseudo-rapidities, $\Delta|\eta| = |\eta_t| - |\eta_{\bar{t}}|$. A comment on the difference

in size of asymmetries for $pp \rightarrow t\bar{t}W^+$ and $pp \rightarrow t\bar{t}W^-$ is in order. The asymmetries are larger for $pp \rightarrow t\bar{t}W^+$ than for $pp \rightarrow t\bar{t}W^-$. Otherwise, however, they behave similarly. As pointed out in Ref. [7] this can be understood by applying an argument based on parton luminosities. At the LO the $t\bar{t}W^+$ process is produced predominantly via $u\bar{d}$ whereas for $t\bar{t}W^-$ the $\bar{u}d$ subprocess is the most relevant one. The longitudinal momenta of the initial partons are on average $p_u > p_d > p_{\bar{u}} \approx p_{\bar{d}}$. In both cases the momentum of the top and anti-top quarks is connected to the momentum of the q and $\bar{q}$ respectively. The large longitudinal momentum transferred to the top quark from the initial u quark in the $t\bar{t}W^+$ case increases the corresponding $|y_t|$ value. Consequently, the charge asymmetry of the top quark is enhanced compared to the one calculated for $t\bar{t}W^-$. When analysing the combined results for $pp \rightarrow t\bar{t}W^{\pm}$ we can observe that the theoretical uncertainties due to the scale dependence reach up to 15%. The scale choice plays no role here as for $\mu_0 = m_t + m_W/2$ and $\mu_0 = H_T/3$ similar results are obtained.

6 Differential and cumulative asymmetry

In this part of the paper we present predictions for differential A_c^{ℓ} asymmetry with respect to the following observables: transverse momentum of the two charged leptons, $p_T(\ell_t \ell_{\bar{t}})$, rapidity of the two charged leptons, $|y(\ell_t \ell_{\bar{t}})|$, and invariant mass of the two charged leptons, $M(\ell_t \ell_{\bar{t}})$, where $\ell_t \ell_{\bar{t}}$ originate from the $t\bar{t}$ pair. The differential results are given using the unexpanded definition from Eq. (18). We also present predictions for cumulative asymmetries, that are closely related to the corresponding differential asymmetries. One can employ the same definition as in Eq. (18), however, this time for a given value of the kinematic variable for which we compute the asymmetry the bin ranges from zero to that value. Even though differential and cumulative asymmetries contain the same information, the latter one behaves better simply because it is more inclusive, i.e. the higher order corrections are distributed more uniformly over the whole kinematic range. In addition, the cumulative asymmetry should give the integrated one in the last bin assuming that the plotted range of the corresponding differential distribution covers the whole available phase space. In practice, we shall see that if the left-over phase space region is negligible the integrated asymmetry can be recovered very accurately. Let us note that differential asymmetries have been studied at the LHC for the $pp \rightarrow t\bar{t}$ production process by both experimental collaborations ALTAS and CMS, see e.g. [92,95].

In Fig. 7 the $p_T(\ell_t \ell_{\bar{t}})$-dependent differential and cumulative A_c^{ℓ} asymmetry at NLO QCD for $pp \rightarrow t\bar{t}W^{\pm}$ in multi-lepton channel at the LHC with $\sqrt{s} = 13$ TeV is displayed. Various approaches for the modelling of the top quark pro-
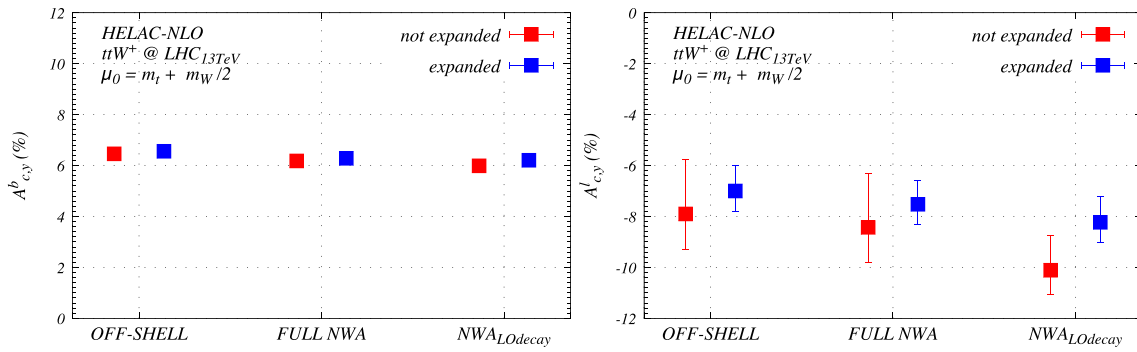
Fig. 6 As in Fig. 5 but for A_c^b and A_c^ℓ

Table 5 As in Table 3 but for $\mu_0 = H_T/3$

$t\bar{t}W^+$ $\mu_0 = H_T/3$	OFF- SHELL	FULL NWA	NWA$_{LOdecay}$
$A_{c,y}^t$ [%]	$2.36(8)^{+1.19\,(50\%)}_{-0.77\,(33\%)}$	$1.93(5)^{+1.23\,(64\%)}_{-0.72\,(37\%)}$	$1.11(3)^{+0.55\,(49\%)}_{-0.53\,(48\%)}$
$A_{c,exp,y}^t$ [%]	$2.66(10)^{+0.38\,(14\%)}_{-0.34\,(13\%)}$	$2.20(5)^{+0.45\,(20\%)}_{-0.31\,(14\%)}$	$2.08(5)^{+0.24\,(11\%)}_{-0.40\,(19\%)}$
$A_{c,\eta}^t$ [%]	$3.46(9)^{+1.41\,(41\%)}_{-0.90\,(26\%)}$	$3.02(5)^{+1.44\,(48\%)}_{-0.93\,(31\%)}$	$1.42(4)^{+0.59\,(41\%)}_{-0.56\,(39\%)}$
$A_{c,exp,\eta}^t$ [%]	$3.81(10)^{+0.46\,(12\%)}_{-0.40\,(10\%)}$	$3.36(5)^{+0.48\,(14\%)}_{-0.43\,(13\%)}$	$2.42(5)^{+0.27\,(11\%)}_{-0.44\,(18\%)}$

Table 6 As in Table 4 but for $\mu_0 = H_T/3$

$t\bar{t}W^+$ $\mu_0 = H_T/3$	OFF- SHELL	FULL NWA	NWA$_{LOdecay}$
$A_{c,y}^b$ [%]	$6.48(9)^{+0.04\,(0.6\%)}_{-0.05\,(0.8\%)}$	$6.16(4)^{+0.07\,(1.1\%)}_{-0.01\,(0.2\%)}$	$6.05(3)^{+0.02\,(0.3\%)}_{-0.01\,(0.2\%)}$
$A_{c,exp,y}^b$ [%]	$6.53(10)^{+0.03\,(0.4\%)}_{-0.08\,(1.2\%)}$	$6.21(5)^{+0.09\,(1.4\%)}_{-0.05\,(0.8\%)}$	$6.23(5)^{+0.02\,(0.3\%)}_{-0.04\,(0.6\%)}$
$A_{c,y}^\ell$ [%]	$-7.46(11)^{+2.46\,(33\%)}_{-1.55\,(21\%)}$	$-7.94(4)^{+2.45\,(31\%)}_{-1.54\,(19\%)}$	$-9.81(4)^{+1.46\,(15\%)}_{-1.03\,(10\%)}$
$A_{c,exp,y}^\ell$ [%]	$-6.93(13)^{+1.01\,(14\%)}_{-0.81\,(12\%)}$	$-7.43(5)^{+0.99\,(13\%)}_{-0.79\,(11\%)}$	$-8.14(5)^{+1.00\,(12\%)}_{-0.81\,(10\%)}$

Table 7 Expanded A_c^t, A_c^ℓ and A_c^b at NLO in QCD for $pp \to t\bar{t}W^+$ and $pp \to t\bar{t}W^-$ in the multi-lepton channel at the LHC with $\sqrt{s} = 13$ TeV. Results are obtained with the full off-shell effects included. Also given are combined results for $pp \to t\bar{t}W^\pm$ and theoretical uncertainties. The NNPDF3.0 PDF set is employed and $\mu_R = \mu_F = \mu_0$ where $\mu_0 = m_t + m_W/2$ and $\mu_0 = H_T/3$

| $\mu_0 = m_t + m_W/2$	$t\bar{t}W^+$	$t\bar{t}W^-$	$t\bar{t}W^\pm$
$A_{c,exp,y}^t$ [%]	$2.62^{+0.39\,(15\%)}_{-0.34\,(13\%)}$	$1.97^{+0.31\,(16\%)}_{-0.25\,(13\%)}$	$2.40^{+0.37\,(15\%)}_{-0.31\,(13\%)}$
$A_{c,exp,\eta}^t$ [%]	$3.70^{+0.46\,(12\%)}_{-0.40\,(11\%)}$	$1.31^{+0.32\,(24\%)}_{-0.25\,(19\%)}$	$2.87^{+0.41\,(14\%)}_{-0.35\,(12\%)}$
$A_{c,exp,y}^b$ [%]	$6.56^{+0.02\,(0.3\%)}_{-0.07\,(1.1\%)}$	$4.80^{+0.05\,(1.0\%)}_{-0.05\,(1.0\%)}$	$5.93^{+0.03\,(0.5\%)}_{-0.08\,(1.3\%)}$
$A_{c,exp,y}^\ell$ [%]	$-7.00^{+1.00\,(14\%)}_{-0.80\,(11\%)}$	$-5.68^{+0.78\,(14\%)}_{-0.61\,(11\%)}$	$-6.51^{+0.93\,(14\%)}_{-0.74\,(11\%)}$
$\mu_0 = H_T/3$	$t\bar{t}W^+$	$t\bar{t}W^-$	$t\bar{t}W^\pm$
$A_{c,exp,y}^t$ [%]	$2.66^{+0.38\,(14\%)}_{-0.34\,(13\%)}$	$2.05^{+0.33\,(16\%)}_{-0.27\,(13\%)}$	$2.45^{+0.37\,(15\%)}_{-0.31\,(13\%)}$
$A_{c,exp,\eta}^t$ [%]	$3.81^{+0.46\,(12\%)}_{-0.40\,(10\%)}$	$1.31^{+0.33\,(25\%)}_{-0.26\,(20\%)}$	$2.94^{+0.42\,(14\%)}_{-0.35\,(12\%)}$
$A_{c,exp,y}^b$ [%]	$6.53^{+0.03\,(0.4\%)}_{-0.08\,(1.2\%)}$	$4.80^{+0.06\,(1.2\%)}_{-0.11\,(2.3\%)}$	$5.91^{+0.04\,(0.7\%)}_{-0.09\,(1.5\%)}$
$A_{c,exp,y}^\ell$ [%]	$-6.93^{+1.01\,(14\%)}_{-0.81\,(12\%)}$	$-5.67^{+0.81\,(14\%)}_{-0.63\,(11\%)}$	$-6.46^{+0.95\,(15\%)}_{-0.75\,(12\%)}$
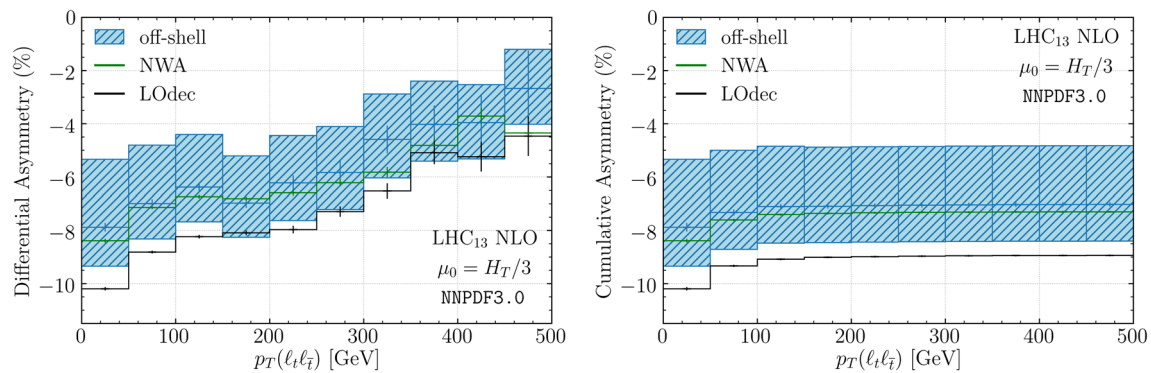
Fig. 7 The $p_T(\ell_t \ell_{\bar{t}})$-dependent differential (left panel) and cumulative (right panel) A_c^ℓ asymmetry at NLO QCD for $pp \to t\bar{t}W^\pm$ in the multi-lepton channel at the LHC with $\sqrt{s} = 13$ TeV. Various approaches for the modelling of the top quark production and decays are considered. Also given are theoretical uncertainties for the full off-shell case. For all approaches Monte Carlo errors are provided for both differential and cumulative asymmetries. The NNPDF3.0 PDF set is employed and $\mu_R = \mu_F = \mu_0$ where $\mu_0 = H_T/3$

duction and decays are considered. Also given are theoretical uncertainties for the full off-shell case. For all approaches Monte Carlo integration errors are provided for both differential and cumulative asymmetries. For the $p_T(\ell_t \ell_{\bar{t}})$-dependent differential asymmetry the MC error is smaller than the theoretical one in all bins but the last. In the last bin both uncertainties are comparable in size. The NNPDF3.0 PDF set is employed and μ_R as well as μ_F are set to the common value $\mu_R = \mu_F = \mu_0 = H_T/3$. For the differential A_c^ℓ asymmetry the difference between the full off-shell result and the full NWA case is in the $5\% - 30\%$ range depending on the bin, yet within theoretical uncertainties, that are of the order of 30%. We notice that this is not the case for the last bin where the top quark off-shell effects affect A_c^ℓ substantially. Specifically, they are above 60%. Also theoretical uncertainties increase in that bin and are of the order of 50%. Both values, however, are harder to specify more precisely due to the large statistical errors. The $\mathrm{NWA_{LOdecay}}$ case, on the other hand, is outside the scale dependence bands almost in the whole plotted range. The difference to the full off-shell approach is larger, even up to 70%. A similar effect is also visible for the cumulative asymmetry where a rather constant 30% difference is noted for the $\mathrm{NWA_{LOdecay}}$ case. Finally, we note that the last bin of the cumulative A_c^ℓ asymmetry gives $A_c^\ell = -7.02(8)$ for the complete off-shell case, $A_c^\ell = -7.30(4)$ for the full NWA and $A_c^\ell = -8.94(3)$ for the $\mathrm{NWA_{LOdecay}}$ case, where in parentheses the MC error is displayed. All three results are indeed in perfect agreement within the MC errors with the corresponding results for the unexpanded leptonic charge asymmetry for the combined $pp \to t\bar{t}W^\pm$ process.

Similar observations can be made for the other two differential and cumulative A_c^ℓ asymmetries. The $|y(\ell_t \ell_{\bar{t}})|$- and $M(\ell_t \ell_{\bar{t}})$-dependent versions of A_c^ℓ are exhibited in Fig. 8 and Fig. 9 respectively. Since in each case the y axis is chosen to be the same for the differential and cumulative version of A_c^ℓ we can distinctly observe that the cumulative asymmetry has smaller fluctuations of the theoretical errors and it is smoother due to better statistical errors. Taking the differential $M(\ell_t \ell_{\bar{t}})$-dependent version of A_c^ℓ as an example we observe large, of the order of 100%, theoretical uncertainties at the tails. On the other hand, the cumulative $M(\ell_t \ell_{\bar{t}})$-dependent A_c^ℓ asymmetry has stable theoretical uncertainties of the order of 30% in the whole plotted range.

We summarise by noting, that several processes beyond the SM can alter A_c, see e.g. [7,96–99], either with anomalous vector or axial-vector couplings or via interference with SM processes. Different models also predict different asymmetries as a function of the invariant mass and the transverse momentum, see e.g. [100]. Of course due to the much smaller cross section the $pp \to t\bar{t}W^\pm$ process will not replace the use of the asymmetries in $t\bar{t}$ production, however, it can provide a complementary tool as it is uniquely sensitive to the chiral nature of possible new physics that might manifest itself in this channel. This motivates our interest in the top quark charge asymmetry as well as the asymmetries of its decay products and their sensitivity to the top quark production and decay modelling. Furthermore, using our NLO QCD results with the full off-shell effects included, we are able to provide more precise theoretical predictions for A_c^t, A_c^ℓ and A_c^b in the $t\bar{t}W^\pm$ production process at the LHC with $\sqrt{s} = 13$ TeV. Finally, having at hand the full theory with no approximations included we are able to study the real size of theoretical uncertainties due to the scale dependence. In other words to verify whether they are under- or overestimated in the presence of various approximations.
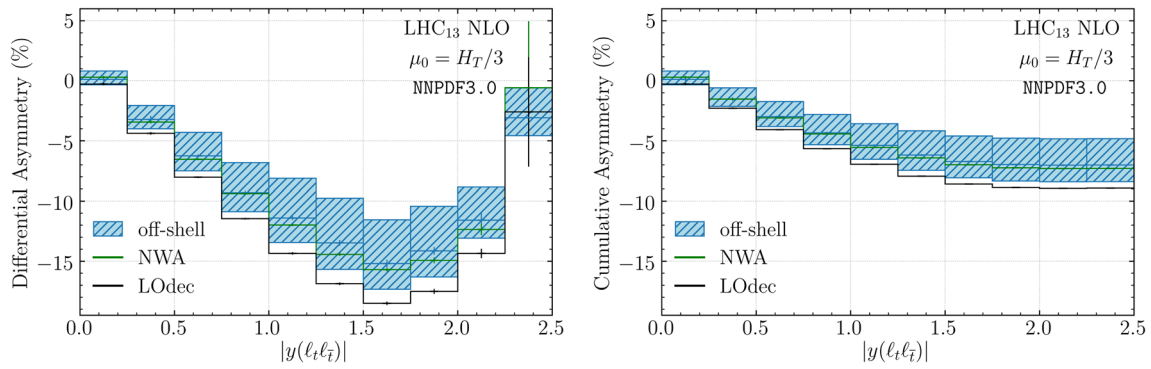
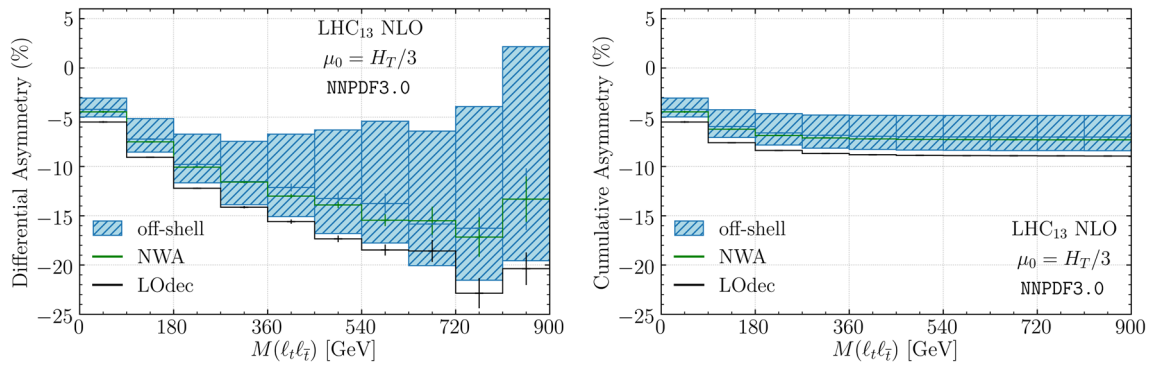**Fig. 8** As in Fig. 7 but for $|y(\ell_t\ell_{\bar{t}})|$

Fig. 9 As in Fig. 7 but for $M(\ell_t\ell_{\bar{t}})$

7 Summary

In this paper we provided the state-of-the-art theoretical predictions for observables, which might be used to constrain numerous new physics scenarios in the $t\bar{t}W^{\pm}$ channel. We considered the $t\bar{t}W^{\pm}$ production process in the multi-lepton decay channel for the LHC Run II energy of $\sqrt{s} = 13$ TeV for which discrepancies in the overall normalisation and in the modelling of the top quark decays have been recently reported by the ATLAS collaboration. Without the need of including terms beyond NLO in the perturbative expansion in α_s we obtained $1\% - 2\%$ theoretical uncertainties due to the scale dependence for this process by calculating the following cross section ratio $\mathcal{R} = \sigma_{t\bar{t}W^+}/\sigma_{t\bar{t}W^-}$. The PDF uncertainties for $\mathcal{R}$ are similar in size. Fully realistic NLO QCD calculations have been employed in our studies for both $t\bar{t}W^+$ and $t\bar{t}W^-$. Specifically, we use $e^+\nu_e\,\mu^-\bar{\nu}_\mu\,e^+\nu_e\,b\bar{b}$ and $e^-\bar{\nu}_e\,\mu^+\nu_\mu\,e^-\bar{\nu}_e\,b\bar{b}$ matrix elements in our NLO QCD calculations. They include all resonant and non-resonant top quark and W gauge boson Feynman diagrams, their interference effects as well as off-shell effects of t and W. We examined the fixed and dynamical scale choice for μ_R and μ_F

to assess their impact on the cross section ratio. We noticed that the scale choice does not play any role for such an inclusive observable. Indeed, although the scale variation is taken correlated in both cases, the fact that the errors come out the same in both cases means that tails of distributions, where the processes show more differences do not matter for the analysis. Otherwise, the error estimate for the fixed scale should be much larger, or the value of the ratio and asymmetries should be shifted outside the error bands. In the next step we examined the impact of the top quark production and decay modelling on the cross section ratio. We observed that the full NWA approach does not modify either the value or the size of the theoretical error for the integrated cross section ratio. Even for the simplified version of the NWA, i.e. for the $\text{NWA}_{\text{LOdecays}}$ case, no changes have been observed. Thus, the $\mathcal{R} = \sigma_{t\bar{t}W^+}/\sigma_{t\bar{t}W^-}$ observable is very stable and insensitive to the details of the modelling of the top quark decay chain. As such, it can be safely exploited at the LHC either for the precision SM measurements or in searches for BSM physics. The $\mathcal{R}$ observable can be used, for example, to provide valuable input for the up and down quark parton distribution functions. In the case of new physics searches

the presence of two same-sign leptons in the final state offers a very interesting signature, that has been highly scrutinised in many new physics models. The latter range from supersymmetry and supergravity to the more specific scenarios with the Majorana neutrinos and the modified Higgs boson sector. Given the final accuracy of $\mathcal{R}$ and its insensitivity to the top quark modelling, the $\mathcal{R}$ observable might be used at the LHC, for example to achieve more stringent limits on the parameter space of these models.

In the second part of the paper we reexamined the top quark charge asymmetry and the charge asymmetries of the top quark decay products for $t\bar{t}W^+$, $t\bar{t}W^-$ and $t\bar{t}W^\pm$ production in the fiducial phase-space regions. Also in this case theoretical predictions with the full off-shell effects were utilised. We presented predictions for the expanded and unexpanded asymmetries. Overall, good agreement has been found for A_c^t, A_c^ℓ and A_c^b when comparing the full off-shell case with the full NWA approach. For the NWA$_{\text{LOdecay}}$ case, however, discrepancies between central values of the asymmetries even up to 2σ have been found. The later fact indicates that NLO QCD corrections to the top quark decays play a crucial role here. Generally, the inclusion of the complete description for the $pp \to t\bar{t}W^\pm$ process in the multi-lepton final state has increased the central values of the asymmetries keeping at the same time the theoretical errors unchanged and below 15%. The scale choice has played no role as for $\mu_0 = m_t + m_W/2$ and $\mu_0 = H_T/3$ similar results have been obtained for A_c^t, A_c^ℓ and A_c^b.

As a bonus of our study, we presented predictions for the differential and cumulative A_c^ℓ asymmetry with respect to $p_T(\ell_t \ell_{\bar{t}})$, $|y(\ell_t \ell_{\bar{t}})|$ and $M(\ell_t \ell_{\bar{t}})$. The advantage of choosing A_c^ℓ lies in the fact that the measurements of the charged leptons are particularly precise at the LHC due to the excellent lepton energy resolution of the ATLAS and CMS detectors. We note here that for these studies the unexpanded version of A_c^ℓ has been examined. Depending on the bin the differences between the full off-shell results and the full NWA ones have been in the 5–30% range. However, this is well within theoretical uncertainties, that are of the order of 30%. On the other hand, large differences have been noticed for the NWA$_{\text{LOdecay}}$ case even up to 70%. Similarly for the cumulative asymmetry the NWA$_{\text{LOdecay}}$ curves are lying outside the uncertainty bands independently of the observable and the considered bin. We would like to add here that even though differential and cumulative asymmetries contain the same information, the latter behaves better simply because it is more inclusive. In other words, the higher order corrections are distributed more uniformly over the whole kinematic range.

Last but not least, we would like to mention at this point that, several BSM physics scenarios can alter the top quark charge asymmetry. Thus, theoretical predictions for the A_c^t, A_c^ℓ and A_c^b observables should be as accurate as possible. Using our NLO QCD results with the full off-shell effects

included not only are we able to provide the state-of-the-art theoretical predictions for A_c^t, A_c^ℓ and A_c^b in the $t\bar{t}W^\pm$ production process but also by the explicit comparison to various NWA approaches we could carefully examine the impact of different top-quark decay modelling accuracies on the scale uncertainties.

Data Availability Statement This manuscript has no associated data or the data will not be deposited. [Authors' comment: All data generated for this study are included in the published article. The detailed numerical data used to produce the distributions shown in the paper are available from the corresponding author on request.]

Appendix A: Kolmogorov–Smirnov test

In Sect. 3 we have only used visual inspection to see whether two given one-dimensional normalised cross section distributions are similar or not. We stress that this is independent of other arguments that we provided to argue for the similarity of the processes. Even though this is an excellent place to start with, we would like to find a more quantitative approach to analyse the issue. In statistics literature several standard procedures exist for this task. Typically, the similarity of histograms is measured by a test statistic. The latter provides the quantitative expression of the distance between the two histograms that are compared. The smaller the distance the more similar are the compared histograms. There are several definitions of the test statistics in specialist literature on

statistical methods. In the following we shall concentrate on the Kolmogorov–Smirnov test (KS test) statistics. The purpose of the (two-sample) KS test is to look for differences in the shape of two one-dimensional probability distributions. It is based on comparing two cumulative distribution functions (CDFs). The KS test reports on the maximum difference between the two CDFs and calculates a p-value from that and the sample sizes. If the two tested histograms are indeed identical then they would have the same CDF. However, in reality two samples that are compared are randomly taken from their corresponding probability distributions. Therefore, even for the two truly identical histograms the corresponding CDFs will be slightly different. We can use this fact to test the two distribution equality by comparing the KS test statistic to 0. If the latter is significantly larger than 0 and close to 1, then we might conclude that the distributions are not equal and the two processes considered are not similar. We begin with the differential cross section distribution for $pp \rightarrow t\bar{t}W^+$ and $pp \rightarrow t\bar{t}W^-$ as a function of the variable x, where x for example is $x = p_{T,e_1}$, $M_{e_1e_2}$. When comparing both histograms, we use the same number of bins. We would like to verify the hypothesis that the two histograms are similar. To this end we calculate the KS test statistics according to

$$\text{KS}_{\text{statistic}} = \sup_x |F^1_{n_1}(x) - F^2_{n_2}(x)|, \tag{A1}$$

where $F^1_{n_1}$ and $F^2_{n_2}$ are the CDFs, n_1 and n_2 are the sizes of the first and second sample respectively and sup is the supremum function. We assume approximately 2000 events for $pp \rightarrow t\bar{t}W^+$ and about 1000 for $pp \rightarrow t\bar{t}W^-$, which correspond to the integrated LHC luminosity of $\mathcal{L} = 500$ fb^{-1} including a lepton-flavour factor of 8. After finding the maximum distance, we use the following condition

$$\sqrt{n}\ \text{KS}_{\text{statistic}} > \lambda(\alpha), \tag{A2}$$

where

$$n = \frac{n_1 \cdot n_2}{n_1 + n_2}, \tag{A3}$$

with $n_1 = 2000$, $n_2 = 1000$ and $\lambda(\alpha)$ is the threshold value that depends on the level of significance α. It can be found from the following condition

$$\mathcal{P}\left(\sqrt{n}\ \text{KS}_{\text{statistic}} > \lambda(\alpha)\right) = 1 - \mathcal{Q}_{\text{KS}}(\lambda(\alpha)) = \alpha, \tag{A4}$$

where $\mathcal{P}$ denotes probability and $\mathcal{Q}_{\text{KS}}(x)$ stands for the Kolmogorov–Smirnov distribution. We reject the hypothesis that the two distributions are similar if

$$\sqrt{n}\ \text{KS}_{\text{statistic}} > \lambda(\alpha), \tag{A5}$$

and accept it when

$$\sqrt{n}\ \text{KS}_{\text{statistic}} \leq \lambda(\alpha). \tag{A6}$$

We would normally start to question the hypothesis of the similarity of the histograms only if we find a difference larger than 2σ (the p-value smaller than 0.0455). If the difference is smaller than 2σ (the p-value larger than 0.0455) then we assume that the two tested distributions are indeed similar. Results that differ more than 3σ (the p-value smaller than 0.0027) can be directly translated into having enough evidence to reject the hypothesis, i.e. saying that there is a real difference between the two samples that are being studied. Note that the KS test does not identify the source of the difference between histograms. It is a robust way of saying that there is a difference, however, the origin of such a difference must be identified by other means.

As the example in Fig. 10 we present the distribution of the KS test statistic for the following NLO QCD differential cross sections: p_{T,e_1}, M_{ee}, H_T^{lep} and ΔR_{ee} for $pp \rightarrow t\bar{t}W^+$ and $pp \rightarrow t\bar{t}W^-$. The total number of tries is set to $N_{tries} = 1000$. All KS test statistic values are distributed within the $0.01 - 0.07$ range, i.e. very close to zero, which suggests that $pp \rightarrow t\bar{t}W^+$ and $pp \rightarrow t\bar{t}W^-$ are indeed correlated. Also shown in Fig. 10 are the distributions of the corresponding p-values for the KS test statistic. We can observe that the p-values are mostly distributed in the vicinity of 1, again supporting the hypothesis that $pp \rightarrow t\bar{t}W^+$ and $pp \rightarrow t\bar{t}W^-$ are highly correlated. We note here, that similar results have been obtained for the kinematics of the b-jet and for the H_T^{vis} observable.

We would like to stress at this point, that for higher integrated luminosity or for an increased number of bins, the sensitivity of the KS test increases as well. As an example we present in Fig. 11 the distribution of p-values for the KS test statistic for the H_T^{vis} observable for $pp \rightarrow t\bar{t}W^+$ and $pp \rightarrow t\bar{t}W^-$. We use four different values for the number of histogram bins, keeping the number of total events fixed for both processes. Specifically, we employ 5, 10, 20 and 40 bins respectively. We can observe that the percentage of N_{tries} with the p-value close to 1 is getting lower as the number of bins increases.

We summarise this part by noting, that there are many test statistics for the comparison of the shapes of two one-dimensional histograms. The most popular are: the Pearson-χ^2 test, the Anderson–Darling test or the Cramer–von-Mises test, see e.g. [101]. Each of these tests has its pros and cons and it is not possible to choose the one test that is the best for all applications. Overall, the more we know about what we really want to compare and test, the more reliable the test we can choose for our particular problem. We have examined all the above-mentioned tests and have decided to use the Kolmogorov–Smirnov test of the equality. The two sample
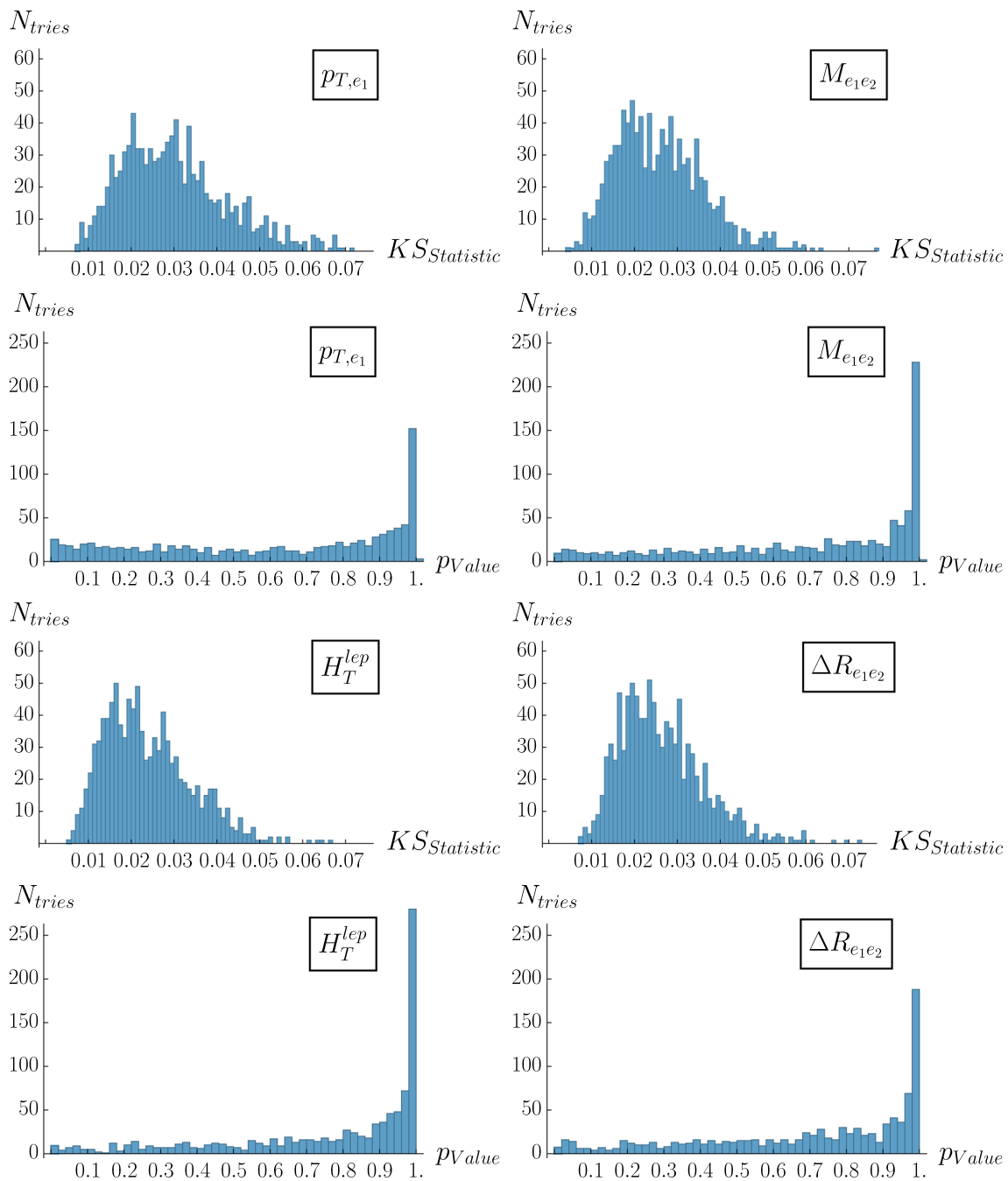
Fig. 10 The distribution of the Kolmogorov–Smirnov test statistic (distance) for the null hypothesis of equality of the histogram shapes. NLO QCD differential cross section distributions for $pp \to t\bar{t}W^+$ and $pp \to t\bar{t}W^-$ in the multi-lepton final state are employed as a function of p_{T,e_1}, $M_{e_1 e_2}$, H_T^{lep} and $\Delta R_{e_1 e_2}$ for the LHC with $\sqrt{s} = 13$ TeV. Also shown are the distributions of the corresponding p-values. The total number of N_{tries} is set to 1000

KS test assumes continuous distributions. It is one of the most general nonparametric[3] tests for comparing two samples, as it is sensitive to differences in shape of the empirical cumulative distribution functions of the two samples. It is also the most robust test as it tests for any violation of the null hypothesis. However, it requires a relatively large number of data points in each bin. We further notice, that the KS test is more sensitive to the regions near the peak of the tested distributions rather than to their tails. For the latter the Anderson–Darling test would do a better job. This observation is very

---

[3] The nonparametric test does not assume that data points are sampled from the Gaussian distribution or any other defined distribution for that matter.
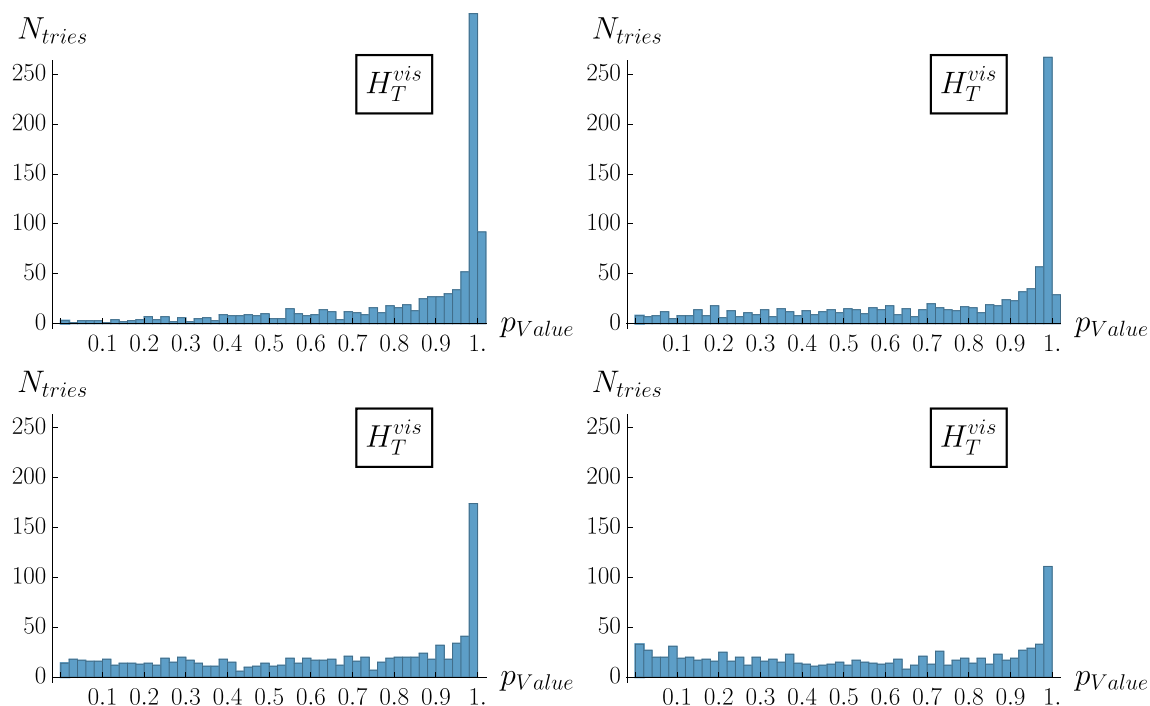
Fig. 11 The distribution of p-values for the Kolmogorov–Smirnov test statistic for the NLO QCD differential cross section for $pp \rightarrow t\bar{t}W^{+}$ and $pp \rightarrow t\bar{t}W^{-}$ in the multi-lepton final state as a function of H_T^{vis} for the LHC with $\sqrt{s} = 13$ TeV. A different number of bins is assumed for each plot, however, the integrated luminosity is kept fixed. Specifically, we use the following four cases: 5 bins (upper left), 10 bins (upper right), 20 bins (lower left) and 40 bins (lower right). The total number of N_{tries} is set to 1000

useful in our case as for many dimensionful observables tails are usually plagued by larger statistical fluctuations and are, therefore, not really reliable for such comparisons.

Finally, we stress that the distributions of observables observed in the two processes are not identical. Hence, the outcome of the test statistic does depend on the number of events. With large numbers of events, the test statistic would obviously discover that the distributions are different. However, we are here interested in the question of "how similar are the distributions?" and not "are the distributions identical?". Quantifying similarity can therefore be done by choosing a number of events. Had we taken processes with very dissimilar distributions the p-value for the same number of events as chosen here, would be much smaller, and we would conclude that the distributions are less similar than in this particular case.

References

1. K. Hagiwara, S. Ishihara, R. Szalapski, D. Zeppenfeld, Phys. Rev. D **48**, 2182 (1993)
2. G.F. Giudice, C. Grojean, A. Pomarol, R. Rattazzi, JHEP **06**, 045 (2007). arXiv:hep-ph/0703164
3. B. Grzadkowski, M. Iskrzynski, M. Misiak, J. Rosiek, JHEP **10**, 085 (2010). arXiv:1008.4884
4. T. Corbett, O.J.P. Eboli, J. Gonzalez-Fraile, M.C. Gonzalez-Garcia, Phys. Rev. D **87**, 015022 (2013). arXiv:1211.4580
5. I. Brivio, M. Trott, Phys. Rep. **793**, 1 (2019). arXiv:1706.08945
6. I. Brivio, S. Bruggisser, F. Maltoni, R. Moutafis, T. Plehn, E. Vryonidou, S. Westhoff, C. Zhang, JHEP **02**, 131 (2020). arXiv:1910.03606
7. F. Maltoni, M. Mangano, I. Tsinikos, M. Zaro, Phys. Lett. B **736**, 252 (2014). arXiv:1406.3262
8. F. Maltoni, D. Pagani, I. Tsinikos, JHEP **02**, 113 (2016). arXiv:1507.05640
9. G. Aad et al. (ATLAS), Eur. Phys. J. C **76**, 259 (2016). arXiv:1602.09058
10. V. Khachatryan et al. (CMS), Eur. Phys. J. C **76**, 439 (2016). arXiv:1605.03171
11. A.M. Sirunyan et al. (CMS), Eur. Phys. J. C **77**, 578 (2017). arXiv:1704.07323
12. M. Aaboud et al. (ATLAS), JHEP **09**, 084 (2017) [Erratum: JHEP **08**, 121 (2019)]. arXiv:1706.03731
13. R. Barnett, J.F. Gunion, H.E. Haber, Phys. Lett. B **315**, 349 (1993). arXiv:hep-ph/9306204
14. M. Guchait, D. Roy, Phys. Rev. D **52**, 133 (1995). arXiv:hep-ph/9412329
15. H. Baer, C.-H. Chen, F. Paige, X. Tata, Phys. Rev. D **53**, 6241 (1996). arXiv:hep-ph/9512383
16. J. Maalampi, N. Romanenko, Phys. Lett. B **532**, 202 (2002). arXiv:hep-ph/0201196

17. H.-C. Cheng, K.T. Matchev, M. Schmaltz, Phys. Rev. D **66**, 056006 (2002). arXiv:hep-ph/0205314

18. H. Dreiner, S. Grab, M. Kramer, M. Trenkel, Phys. Rev. D **75**, 035003 (2007). arXiv:hep-ph/0611195

19. R. Contino, G. Servant, JHEP **06**, 026 (2008). arXiv:0801.1679

20. S. von Buddenbrock, N. Chakrabarty, A.S. Cornell, D. Kar, M. Kumar, T. Mandal, B. Mellado, B. Mukhopadhyaya, R.G. Reed, X. Ruan, Eur. Phys. J. C **76**, 580 (2016). arXiv:1606.01674

21. S. von Buddenbrock, A.S. Cornell, A. Fadol, M. Kumar, B. Mellado, X. Ruan, J. Phys. G **45**, 115003 (2018). arXiv:1711.07874

22. S. von Buddenbrock, A.S. Cornell, E.D. Iarilala, M. Kumar, B. Mellado, X. Ruan, E.M. Shrif, J. Phys. G **46**, 115001 (2019). arXiv:1809.06344

23. S. Buddenbrock, A.S. Cornell, Y. Fang, A. Fadol Mohammed, M. Kumar, B. Mellado, K.G. Tomiwa, JHEP **10**, 157 (2019). arXiv:1901.05300

24. F.M.L. Almeida Jr., Y. do Amaral Coutinho, J.A. Martins Simoes, P. Queiroz Filho, C. Porto, Phys. Lett. B **400**, 331 (1997). arXiv:hep-ph/9703441

25. Y. Bai, Z. Han, JHEP **04**, 056 (2009). arXiv:0809.4487

26. ATLAS-CONF-2019-045 (2019). https://inspirehep.net/literature/1759582

27. G. Aad et al. (ATLAS) (2020) arXiv:2007.14858

28. M. Aaboud et al. (ATLAS), Eur. Phys. J. C **77**, 40 (2017). arXiv:1609.01599

29. A.M. Sirunyan et al. (CMS), JHEP **08**, 011 (2018). arXiv:1711.02547

30. M. Aaboud et al. (ATLAS), Phys. Rev. D **99**, 072009 (2019). arXiv:1901.03584

31. J.M. Campbell, R. Ellis, JHEP **07**, 052 (2012). arXiv:1204.5678

32. G. Bevilacqua, H.-Y. Bi, H.B. Hartanto, M. Kraus, M. Worek, JHEP **08**, 043 (2020a). arXiv:2005.09427

33. A. Denner, G. Pelliccioli (2020) arXiv:2007.12089

34. R. Frederix, I. Tsinikos, Eur. Phys. J. C **80**, 803 (2020). arXiv:2004.09552

35. S. Frixione, B.R. Webber, JHEP **06**, 029 (2002). arXiv:hep-ph/0204244

36. S. Frixione, P. Nason, B.R. Webber, JHEP **08**, 007 (2003). arXiv:hep-ph/0305252

37. T. Sjöstrand, S. Ask, J.R. Christiansen, R. Corke, N. Desai, P. Ilten, S. Mrenna, S. Prestel, C.O. Rasmussen, P.Z. Skands, Comput. Phys. Commun. **191**, 159 (2015). arXiv:1410.3012

38. J. Alwall, R. Frederix, S. Frixione, V. Hirschi, F. Maltoni, O. Mattelaer, H.S. Shao, T. Stelzer, P. Torrielli, M. Zaro, JHEP **07**, 079 (2014). arXiv:1405.0301

39. R. Frederix, S. Frixione, V. Hirschi, D. Pagani, H.S. Shao, M. Zaro, JHEP **07**, 185 (2018a). arXiv:1804.10017

40. P. Artoisenet, R. Frederix, O. Mattelaer, R. Rietkerk, JHEP **03**, 015 (2013). arXiv:1212.3460

41. A. Denner, S. Dittmaier, S. Kallweit, S. Pozzorini, Phys. Rev. Lett. **106**, 052001 (2011). arXiv:1012.3975

42. G. Bevilacqua, M. Czakon, A. van Hameren, C.G. Papadopoulos, M. Worek, JHEP **02**, 083 (2011). arXiv:1012.4230

43. A. Denner, S. Dittmaier, S. Kallweit, S. Pozzorini, JHEP **10**, 110 (2012). arXiv:1207.5018

44. A. Denner, M. Pellen, JHEP **02**, 013 (2018). arXiv:1711.10359

45. G. Bevilacqua, H. Hartanto, M. Kraus, M. Worek, Phys. Rev. Lett. **116**, 052003 (2016). arXiv:1509.09242

46. G. Bevilacqua, H. Hartanto, M. Kraus, M. Worek, JHEP **11**, 098 (2016b). arXiv:1609.01659

47. A. Denner, R. Feger, JHEP **11**, 209 (2015). arXiv:1506.07448

48. G. Bevilacqua, H. Hartanto, M. Kraus, T. Weber, M. Worek, JHEP **10**, 158 (2018). arXiv:1803.09916

49. G. Bevilacqua, H. Hartanto, M. Kraus, T. Weber, M. Worek, JHEP **11**, 001 (2019). arXiv:1907.09359

50. A. Denner, J.-N. Lang, M. Pellen (2020) arXiv:2008.00918

51. M. Garzelli, A. Kardos, C. Papadopoulos, Z. Trocsanyi, JHEP **11**, 056 (2012). arXiv:1208.2665

52. S. von Buddenbrock, R. Ruiz, B. Mellado (2020) arXiv:2009.00032

53. F.F. Cordero, M. Kraus, L. Reina (2021) arXiv:2101.11808

54. S. Frixione, V. Hirschi, D. Pagani, H.S. Shao, M. Zaro, JHEP **06**, 184 (2015). arXiv:1504.03446

55. J.A. Dror, M. Farina, E. Salvioni, J. Serra, JHEP **01**, 071 (2016). arXiv:1511.03674

56. R. Frederix, D. Pagani, M. Zaro, JHEP **02**, 031 (2018b). arXiv:1711.02116

57. H.T. Li, C.S. Li, S.A. Li, Phys. Rev. D **90**, 094009 (2014). arXiv:1409.1460

58. A. Broggio, A. Ferroglia, G. Ossola, B.D. Pecjak, JHEP **09**, 089 (2016). arXiv:1607.05303

59. A. Kulesza, L. Motyka, D. Schwartländer, T. Stebel, V. Theeuwes, Eur. Phys. J. C **79**, 249 (2019). arXiv:1812.08622

60. A. Broggio, A. Ferroglia, R. Frederix, D. Pagani, B.D. Pecjak, I. Tsinikos, JHEP **08**, 039 (2019). arXiv:1907.04343

61. A. Kulesza, L. Motyka, D. Schwartländer, T. Stebel, V. Theeuwes, Eur. Phys. J. C **80**, 428 (2020). arXiv:2001.03031

62. A. Denner, G. Pelliccioli (2021) arXiv:2102.03246

63. G. Bevilacqua, M. Czakon, M. Garzelli, A. van Hameren, A. Kardos, C. Papadopoulos, R. Pittau, M. Worek, Comput. Phys. Commun. **184**, 986 (2013a). arXiv:1110.1499

64. A. van Hameren, C. Papadopoulos, R. Pittau, JHEP **09**, 106 (2009). arXiv:0903.4665

65. G. Ossola, C.G. Papadopoulos, R. Pittau, JHEP **03**, 042 (2008). arXiv:0711.3596

66. M. Czakon, C. Papadopoulos, M. Worek, JHEP **08**, 085 (2009). arXiv:0905.0883

67. G. Bevilacqua, M. Czakon, M. Kubocz, M. Worek, JHEP **10**, 204 (2013b). arXiv:1308.5605

68. A. van Hameren (2010) arXiv:1003.4953

69. J. Butterworth et al., J. Phys. G **43**, 023001 (2016). arXiv:1510.03865

70. R.D. Ball et al., NNPDF. JHEP **04**, 040 (2015). arXiv:1410.8849

71. A. Buckley, J. Ferrando, S. Lloyd, K. Nordstrom, B. Page, M. Ruefenacht, M. Schoenherr, G. Watt, Eur. Phys. J. C **75**, 132 (2015). arXiv:1412.7420

72. M. Cacciari, G.P. Salam, G. Soyez, JHEP **04**, 063 (2008). arXiv:0802.1189

73. G. Bevilacqua, M. Worek, JHEP **07**, 135 (2014). arXiv:1403.2046

74. D. Krohn, M.D. Schwartz, T. Lin, W.J. Waalewijn, Phys. Rev. Lett. **110**, 212001 (2013). arXiv:1209.2421

75. W.J. Waalewijn, Phys. Rev. D **86**, 094030 (2012). arXiv:1209.3019

76. ATL-PHYS-PROC-2017-017 (2017). https://inspirehep.net/literature/1512998

77. ATLAS-CONF-2018-022 (2018). https://atlas.web.cern.ch/Atlas/GROUPS/PHYSICS/CONFNOTES/ATLAS-CONF-2018-022/

78. M. Czakon, Phys. Lett. B **693**, 259 (2010). arXiv:1005.0274

79. M. Czakon, Nucl. Phys. B **849**, 250 (2011). arXiv:1101.0642

80. M. Czakon, D. Heymes, Nucl. Phys. B **890**, 152 (2014). arXiv:1408.2500

81. M. Czakon, A. van Hameren, A. Mitov, R. Poncelet, JHEP **10**, 262 (2019). arXiv:1907.12911

82. C. Duhr, F. Dulat, B. Mistlberger, JHEP **11**, 143 (2020). arXiv:2007.13313

83. W. Bernreuther, Z.-G. Si, Phys. Rev. D **86**, 034026 (2012). arXiv:1205.6580

84. M. Czakon, D. Heymes, A. Mitov, D. Pagani, I. Tsinikos, M. Zaro, Phys. Rev. D **98**, 014003 (2018). arXiv:1711.03945

85. G. Bevilacqua, H. Hartanto, M. Kraus, T. Weber, M. Worek, JHEP **03**, 154 (2020b). arXiv:1912.09999

86. M. Czakon, P. Fiedler, A. Mitov, Phys. Rev. Lett. **115**, 052001 (2015). arXiv:1411.3007
87. M. Czakon, P. Fiedler, D. Heymes, A. Mitov, JHEP **05**, 034 (2016). arXiv:1601.05375
88. S. Chatrchyan et al. (CMS) Phys. Lett. B **709**, 28 (2012). arXiv:1112.5100
89. G. Aad et al. (ATLAS), Eur. Phys. J. C **72**, 2039 (2012). arXiv:1203.4211
90. V. Khachatryan et al. (CMS), Phys. Lett. B **760**, 365 (2016). arXiv:1603.06221
91. G. Aad et al. (ATLAS), Phys. Rev. D **94**, 032006 (2016). arXiv:1604.05538
92. M. Aaboud et al. (ATLAS, CMS), JHEP **04**, 033 (2018). arXiv:1709.05327
93. Tech. Rep. ATLAS-CONF-2019-026, CERN, Geneva (2019). http://cds.cern.ch/record/2682109
94. G. Corcella, I.G. Knowles, G. Marchesini, S. Moretti, K. Odagiri, P. Richardson, M.H. Seymour, B.R. Webber, JHEP **01**, 010 (2001). arXiv:hep-ph/0011363
95. V. Khachatryan et al. (CMS), Phys. Lett. B **757**, 154 (2016). arXiv:1507.03119
96. S. Jung, A. Pierce, J.D. Wells, Phys. Rev. D **83**, 114039 (2011). arXiv:1103.4835
97. P. Ferrario, G. Rodrigo, Phys. Rev. D **78**, 094018 (2008). arXiv:0809.3354
98. J. Aguilar-Saavedra, M. Perez-Victoria, Phys. Rev. D **84**, 115013 (2011). arXiv:1105.4606
99. E. Alvarez, A. Juste, M. Szewc, T. Vazquez Schroeder (2020) arXiv:2011.06514
100. J. Aguilar-Saavedra, M. Perez-Victoria, Phys. Lett. B **705**, 228 (2011b). arXiv:1107.2120
101. F.C. Porter (2008) arXiv:0804.0380